THE UNIVERSITY OF
WARWICK

AUTHOR: **Oliver Dunbar** DEGREE: **MSc**

TITLE: **Knot energies in the numerical detection and prevention of self-intersecting moving membranes**

DATE OF DEPOSIT: .....

I agree that this thesis shall be available in accordance with the regulations governing the University of Warwick theses.

I agree that the summary of this thesis may be submitted for publication.

I **agree** that the thesis may be photocopied (single copies for study purposes only).

Theses with no restriction on photocopying will also be made available to the British Library for microfilming. The British Library may supply copies to individuals or libraries. subject to a statement from them that the copy is supplied for non-publishing purposes. All copies supplied by the British Library will carry the following statement:

> "Attention is drawn to the fact that the copyright of this thesis rests with its author. This copy of the thesis has been supplied on the condition that anyone who consults it is understood to recognise that its copyright rests with its author and that no quotation from the thesis and no information derived from it may be published without the author's written consent."

AUTHOR'S SIGNATURE: .....

USER'S DECLARATION

1. I undertake not to quote or make use of any information from this thesis without making acknowledgement to the author.
2. I further undertake to allow no-one else to use this thesis while it is in my care.

DATE SIGNATURE ADDRESS

.....

.....

.....

.....

.....

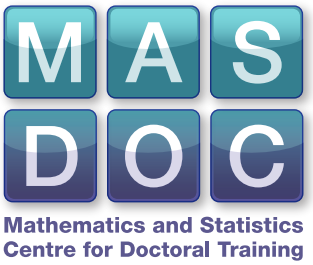

Knot energies in the numerical detection and prevention of self-intersecting moving membranes

by

Oliver Dunbar

Thesis

Submitted for the degree of

Master of Science

Mathematics Institute

The University of Warwick

August 2014

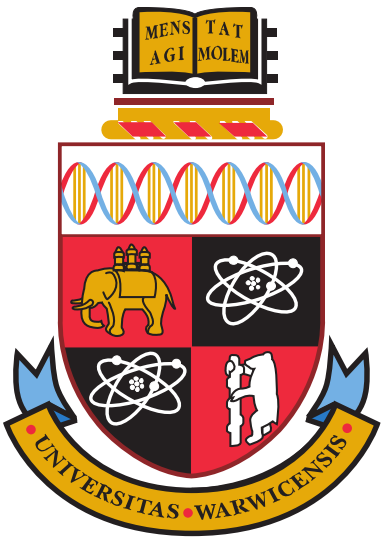

Contents

List of Figures

Acknowledgments

I would like to acknowledge those who have made this thesis possible. Firstly my supervisors Björn Stinner and Andreas Dedner who have first constructed and then supported my project throughout.

Secondly thanks to EPSRC, and MASDOC who provided the funding and environment, in which I could work efficiently and comfortably.

Finally to the statistics department which has continually satisfied my thirst for caffeine throughout my work period, and to Jake Dunn who helped with proof reading.

Declarations

I, Oliver Dunbar, to the best of my knowledge have presented only my original work and the products of my collaboration with Dr Björn Stinner, unless specifically referenced or cited in the bibliography. I will also declare that the work produced here has not been submitted for any other degree or qualification or at any other university.

Abstract

This thesis aims to study the effect implementing a knot energy, to detect and possibly prevent self intersection of an evolving membrane with motion coupled to a surface advection diffusion equation. We first study the famous Möbius knot energy on smooth curves, using quadrature theory to analyse its convergence, and smoothing techniques to improve this. We then construct a discretisation of the energy, generalised from the proposed discretisation by Scholtes, to an energy which can be implemented on unknown curves and study its convergence and methods of increasing computational efficiency. We introduce a SFEM model proposed by Elliot and Dziuk for a quantity on the membrane and couple this to one of two evolution schemes, created by Dziuk and the other by Barrett-Garcke-Nürnberg. Inserting the discretised knot energy, we then compare effectiveness of the different methods of calculating the energy discretisation in these frameworks for detecting self intersections. Finally we propose and implement briefly a possible method of prevention of these membrane self intersections.

Chapter 1

Introduction

1.1 Motivation

Cell motility is the ability for biological (in this case unicellular) organisms to move in a coordinated way due to the presence of nearby stimuli. It is an important process to understand, as even single cell motility encapsulates biological phenomena such as metastasis of cancer, axon guidance, tissue regeneration and embryotic growth.

In essence the movement can be classified into the detection of the stimulus; polarisation - that is the rearranging of chemical concentrations in the cell to attain a "direction" of future movement; then the movement in the required direction that is fueled by concentrations of chemicals distributed across the cell membranes surface. Mathematically we can model the motility using geometric equations for the shape of the cell membrane coupled to surface PDEs for the cell chemistry on the membrane itself, see [8] with specific application to chemotaxis and pseudopod driven migration.

During numerical experiments unphysical phenoma is sometimes observed, one of these specifically is self-intersection of the membrane. One can imagine two attractive stimuli either side of the cell, and the alignment may cause movement in both directions leading to a 'stretching out' of the cell into a thin body, and the boundary membrane may be so close as to touch or even cross in numerical approximation. The aims of this paper will be to (a) detect these self-intersections with the possible further research into techniques of (b) prevention the self-intersections from occuring.

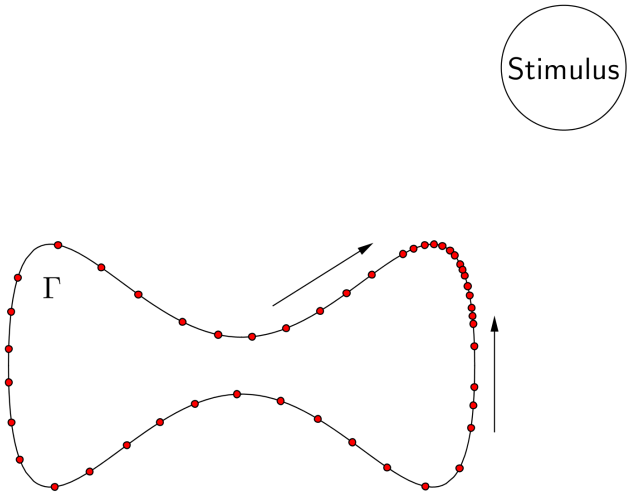

Figure 1.1: *Illustration of chemical distribution across the cell boundary due to a stimulus*

1.2 Outline

We begin with the central quantity of the project, which is the study of the Möbius energy and its discretisation. This energy is a continuous functional, constructed in such a way that if it is a function of a smooth embedded curve the energy will be a small positive quantity (in fact the circle is a minimiser), however as a curve comes close to self-intersection, the value of the energy will explode. This energy was first used to study these detections in [15]. We use quadrature rules to calculate this energy for a given fixed curve and analyse the convergence and discuss how different rates can be attained.

We wish to discretise the integrand of the energy functional, so we must also consider a choice of its discretisation: earlier work in this area can be found in [18] and [17]. Previous research has been more concerned with topological properties of the discrete energy, and thus we are required to modify and generalise from these more algerbraically focused objects. In particular the aim for this chapter is to create a modified Möbius energy which can be calculated efficiently and accurately, on a curve with very little information. Specifically we calculate here on a piecewise linear polynomial approximation to the curve of interest. We predict convergence

rates of the approximations, by analysing regularity of the integrand, and we apply techniques such as cutting off and smoothing or alternative calculation methods. These are then implemented numerically to see if we can improve on the previous research available.

After working with fixed curves we discuss an important model and primary motivation for our work, that is, the model for the cell that was proposed in [8], showing derivations and discretisations. The equations governing the chemical concentrations on the surface of the membrane itself are given by a surface PDE. We look at the mass conservation with source terms of a single chemical (possibly corresponding to the protein 'Actin' that drives the polymerisation reactions causing cell extensions and retractions) - this derivation can be studied in more detail in [6] and [7].

The other half of this model is dedicated to representing the membrane itself, which is modelled by a geometric evolution law governed by curvature flow. This represents the surface tension of the cell membrane, causing it to constantly wish to be as short as possible. In order to prevent the shrinking of our cell volume to zero, and to govern the motion of the cell we also include a forcing term into these equations. We have study two such models proposed in [4] [1]

Next we implement this energy within the numerical schemes for our cell membrane, and highlight some issues that needed to be overcome during this stage. In particular different calculations of the energy - such as introduction of cutoff functions or using a scheme based on equidistribution. We also observe the different effects of the two evolution schemes - for example the BGN method will equidistribute points, whereas Dziuks method enforces motion in only a normal direction to the surface. Studying efficiency of the schemes also plays a large role and we comment on the reduction of computational complexity in this chapter within numerical simulations.

The next chapter gives some brief research and calculations (to reflect the analysis and implementation of the previous chapters based on the detections of intersections) on the work of preventing the self-intersections. In particular the addition of other force terms into our model that are constructed from the value of our energy function.

Finally we discuss some conclusions of the work, and briefly remark on some open problems.

Chapter 2

The Möbius energy

2.1 Form and simple properties

This project wishes to investigate an unwelcome phenomenon that arises in the context of an evolution model (with a view of application in many other evolutionary systems), which is the occurances of self-intersections. Most systems are designed to model real world scenarios and such intersections of a body tends to indicate unrealistic material properties or perhaps singularities/change of state in a model and thus wish to be at the very least detected if not controlled or avoided.

To observe the intersections we use the well studied Möbius energy, (first used in this context in [15]).

Definition 2.1.1. For any parametrisation of an embedded closed curve $\Gamma \subset \mathbb{R}^2$ by the function $\gamma : [0,1] \to \Gamma$. We define the *geodesic distance* or *arc distance* between two points on the curve, through the respective points in the domain of parametristion, i.e $\forall x, y \in [0,1]$:

$$d_\gamma(x,y) \coloneqq \min\left\{\int_x^y |\gamma'(\theta)|\,\mathrm{d}\theta, \int_0^x |\gamma'(\theta)|\,\mathrm{d}\theta + \int_y^1 |\gamma'(\theta)|\,\mathrm{d}\theta\right\} \quad \Big(\geq |\gamma(x)-\gamma(y)|\Big) \tag{2.1}$$

Definition 2.1.2. we define *the Möbius energy functional* as

$$E(\gamma) = \iint_{[0,1]^2} \left(\frac{1}{|\gamma(x)-\gamma(y)|^2} - \frac{1}{d_\gamma(x,y)^2}\right) |\gamma'(x)||\gamma'(y)|\,\mathrm{d}x\,\mathrm{d}y \tag{2.2}$$

We notice a few basic properties from the structure of the energy functional. Firstly, the integrand is of the form of a difference between a function of the Euclidean distance between any two points, and a function of geodesic distance between

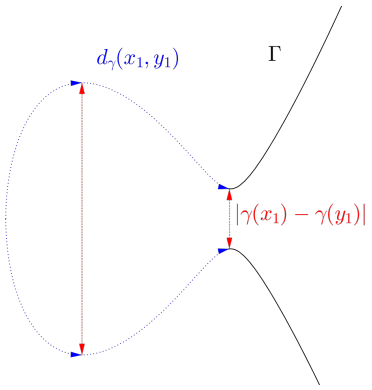

Figure 2.1: *Demonstrating comparison of Euclidean and Geodesic distances on a curve* Γ

two points, it is then naturally weighted via the parametrisation. This difference is what will characterise the 'proximity' to self intersection - which is demonstrated in Figure 2.1. It shows for two pairs of points on the curve, (one far and one close to self intersection) the geodesic distance compared to the Euclidean distance. We see that near self intersection there is a far greater disparity in these two distances, this is thus measured by the integrand. In fact, as self-intersection occurs precisely when the parametrisation becomes noninjective i.e. $\exists\, \tilde{x}, \tilde{y} \in [0,1]$ such that $\gamma(\tilde{x}) = \gamma(\tilde{y})$ but $d_\gamma(\tilde{x}, \tilde{y}) > 0$, this behaviour causes a singularity in (2.2).

Secondly, the inequality in (2.1) shows that this energy is always nonnegative, which always proves a useful inequality.

The energy is scaling invariant, as the $|\gamma'(x)||\gamma'(y)|$ cause the weights of each term to be based on the *proportion* of the length of the curve. It is also invariant under affine transformations i.e if $f : \mathbb{R}^2 \to \mathbb{R}^2$ is an affine transformation ($f(x) = Mx + b$, with $M \in \mathbb{R}^{2\times 2}$, $b \in \mathbb{R}^2$) then E satisfies $E(f \circ \gamma) = E(\gamma)$.

Definition 2.1.3. A function $f : X \to Y$ is *L-bi-lipschitz* if f is an L-lipschitz function and its inverse $f^{-1} : f(X) \to X$ is also L-Lipschitz. equivalently we may write the inequality:

$$\forall\, x, y \in X,\, \exists L > 0 \quad \text{s.t} \quad L^{-1} d_X(x,y) \leq d_Y(f(x), f(y)) \leq L d_X(x,y)$$

Proposition 2.1.1. *[10] Let* $\Gamma \subset \mathbb{R}^2$ *be a closed rectifiable (finite length) curve, and* $\gamma : X \to \mathbb{R}^2$ *an arc length parametrisation. If* $E(\gamma)$ *is finite then* γ *is L-bi-Lipschitz with* L *dependant only upon* $E(\gamma)$*. Moreover,if* γ_n *is a sequence such that* $E(\gamma_n) \to 0$ *as* $n \to \infty$ *then* $L \to 1$ *.*

In fact there are other properties described in [10] that are not detailed here, such as the invariance under Möbius transformations and the energy value can be used to bound the average number of crossings that a planar knot has (using a projection from the curve $\mathbb{R}^3 \to \mathbb{R}^2$ to create the knots), which leads to interesting mathematics in knot theory.

Remark. This is just a subclass of an entire family of knot energies of the form:

$$E^{j,p}(\gamma) = \iint_{[0,1]^2} \left(\frac{1}{|\gamma(x) - \gamma(y)|^j} - \frac{1}{d_\gamma(x,y)^j} \right)^p |\gamma'(x)||\gamma'(y)| \, \mathrm{d}x \, \mathrm{d}y$$

for $(j,p) \in (0,\infty) \times (0,\infty)$. This family has been studied in depth, especially concerning the regularity of the curves for differing exponents (see [14][3]). In these papers the authors show that for $(j-2)p \geq 1$, then the energy is infinite for all smooth closed curves (if $p \geq 1$) and for all polygons (if $jp > 2$) , for $jp < 2$ the energy is finite even during self-intersection of Γ. Also it is shown that if $jp \leq 2$, and $(j-2)p < 1$ then this energy can be finite for curves that are non differentiable, moreover one can choose nondifferentiable curves with energy arbitrarily close to a minimisers energy. (Some necessary and sufficient conditions for bounded $E^{j,p}$ energy may be found in [2])

The choice of $j = 2, p = 1$ is therefore the correct candidate of powers required, by having minimum regularity requirements on γ, and yet still becoming infinite under self-intersection.

2.2 Fixed curve: Analysis

For this section we assume that we are given a parametrisation of a fixed closed curve Γ by $\gamma : [0,1] \to \Gamma$ which is C^∞ - or at least sufficiently smooth for assumptions required by the integrand regularity. We split the unit interval into N pieces and denote $a_i = \frac{i}{N}$.

2.2.1 Quadrature theory

Take a function $F : [0,1] \times [0,1] \to \mathbb{R}$, for which we will consider the integration

$$I(F) \coloneqq \iint_{[0,1]^2} F(x,y) \, \mathrm{d}x \, \mathrm{d}y$$

We impose a *tensor ansatz*, which requires the structure of the meshgrid to be the same in both x and y coordinates. This allows us to retain properties such as symmetry and periodicity of the energy density when using quadrature (or later on,

when discretising). We may then apply quadrature rules such as the midpoint rule in the following manner because of this:

Midpoint quadrature
The midpoint rule is the approximation of a function by a piecewise C^0 polynomial, followed by a weighted summation, given by $\int_a^b f(x)\,\mathrm{d}x \approx (b-a)f(a)$:

$$\int_{a_j}^{a_{j+1}} \int_{a_i}^{a_{i+1}} F(x,y)\,\mathrm{d}x\,\mathrm{d}y \approx \int_{a_j}^{a_{j+1}} (a_{i+1}-a_i)F(a_i,y)\,\mathrm{d}y \approx (a_{j+1}-a_j)(a_{i+1}-a_i)F(a_i,a_j)$$

Overall we sum up to an approximate integral.

$$I_N(F) = \frac{1}{N^2} \sum_{\substack{i\neq j \\ i,j=1}}^{N} F(a_i,a_j)$$

Please note that we remark later on the diagonal terms. Standard numerical analysis then obtains convergence orders based on the degree of accuracy of the quadrature q (here for example $q=0$) and the regularity of the funpction F. In particular we will consider periodic functions (see for example [16])

Proposition 2.2.1. *For a periodic function $F \in W^{k,p}(\mathbb{R}^2)$, $1<p<\infty$, and quadrature rule over exactly one period with exact accuracy up to degree q and meshsize N*

$$|I(F) - I_N(F)| = \mathcal{O}\Big(\frac{1}{N^s}\Big) \qquad \textit{where} \qquad s = \min\{k, q+1\}$$

Thus for an $W^{2,p}$ integrand one may expect that for an order of $\mathcal{O}(\frac{1}{N^2})$ convergence as $N\to\infty$ one may require a higher order quadrature rule such as trapezoidal or Simpson's rule (the latter can be found in the appendix).

Trapezoidal quadrature
The trapezoidal rule is given by $\int_a^b f(x)\,\mathrm{d}x \approx (b-a)\left(\frac{f(a)+f(b)}{2}\right)$, Thus:

$$\int_{a_j}^{a_{j+1}} \int_{a_i}^{a_{i+1}} F(x,y)\,\mathrm{d}x\,\mathrm{d}y \approx \int_{a_j}^{a_{j+1}} (a_{i+1}-a_i)\left(\frac{F(a_i,y)+F(a_{i+1},y)}{2}\right)\,\mathrm{d}y$$

$$\approx \frac{(a_{j+1}-a_j)(a_{i+1}-a_i)}{4}\left[\Big(F(a_i,a_j)+F(a_{i+1},a_j)\Big)+\Big(F(a_i,a_{j+1})+F(a_{i+1},a_{j+1})\Big)\right]$$

by defining $a_{N+1} \coloneqq a_1$ then we represent the discretised integral as follows

$$I_N(F) = \frac{1}{4N^2} \sum_{\substack{i \neq j \\ i,j=1}}^{N} \Big[\Big(F(a_i, a_j) + F(a_{i+1}, a_j) \Big) + \Big(F(a_i, a_{j+1}) + F(a_{i+1}, a_{j+1}) \Big) \Big]$$

We have not yet considered the form of our integrand F, from (2.2) we define

$$F(x, y) \coloneqq \left(\frac{1}{|\gamma(x) - \gamma(y)|^2} - \frac{1}{d_\gamma(x, y)^2} \right) |\gamma'(x)||\gamma'(y)| \tag{2.3}$$

The closedness of Γ and the tensor ansatz of F cause it to have a continuous periodic extension $\overline{F}$ (with periodic cell $[0, 1]^2$), i.e $\overline{F}(x, y) = \overline{F}(x, y + 1) = \overline{F}(x + 1, y)$ $\forall x, y \in \mathbb{R}^2$. Also we gain the property of symmetry about $y = x$ naturally.

As we are integrating over exactly a single periodic cell one may shift this cell by a transformation $(x, y) \mapsto (x + \frac{1}{2}, y + \frac{1}{2})$, before performing the trapezoidal rule. Notice now that the nodes of the trapezoidal rule are exactly the nodes of the midpoint rule on the original domain. This is important as it states that we should see (for a $W^{2,p}$ function) the same convergence rates of $\mathcal{O}(\frac{1}{N^2})$ with the constant quadrature rule or the trapezoidal rule.

Another upshot of the form of our integrand comes from the presence of a singularity along the line $x = y$. As of yet we have not analysed the integrand F and so we have naïvely assign these a value zero, as on a brief inspection we at least see that it is a removable singularity and so the integrand does not explode here.

Remark. for more general results for the accuracy of piecewise polynomial quadrature rules of periodic functions in multiple dimensions one may attempt to generalise those found in [12] and [11].

We now look at the other limiting factor for the convergence order of our energy. That is, the regularity.

2.2.2 Regularity of the integrand

The knot energy is historically considered a more topological or algebraic tool for determining if a curve contains intersections and knots. Therefore there is plenty of documentation of estimates of the curves regularity given that the energy attains certain values or is bounded such as in Proposition 2.1.1. However, less has been said about what happens to the energy's integrand if provided with a curve of certain regularity (As we have seen with quadrature this will certainly become problematic

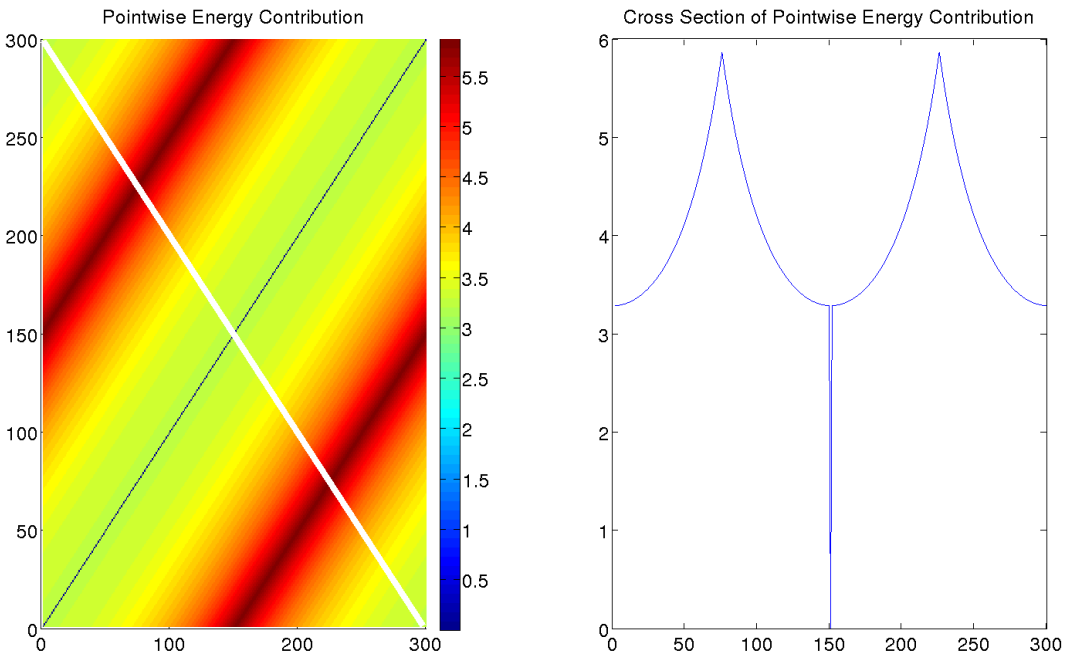

Figure 2.2: *The left: energy density of the exact unit circle, on the right: the cross section plotted along the white line*

for rates of convergence if it is nonsmooth). The main causes for concern in this integrand for a smooth γ are where both the geodesic and Euclidean distances between points are close to 0, and also the effect of the minimum function in d_γ will certainly lead to cusps.

We will consider a specific test example throughout this chapter, where

$$\gamma : [0,1] \to \mathbb{S}^1, \qquad \gamma(t) = \begin{pmatrix} \cos(2\pi t) \\ \sin(2\pi t) \end{pmatrix}$$

the parametrisation of the unit circle, and consider the discretisation given in previous subsections. We wish to consider the most obvious case of where the integrand F may develop problems with its regularity, the convergence of two points together, i.e $x, y \in \mathbb{S}^1$ with $x \to y$.

The Euclidean distance between any two quadrature mesh points on the circle $a_i = \frac{i}{N}$, $a_j = \frac{j}{N}$ is given by:

$$|\gamma(a_i) - \gamma(a_j)|^2 = \left(\cos\left(\frac{2\pi i}{N}\right) - \cos\left(\frac{2\pi j}{N}\right)\right)^2 + \left(\sin\left(\frac{2\pi i}{N}\right) - \sin\left(\frac{2\pi j}{N}\right)\right)^2$$

and the (exact) arclength is given by (wlog $i > j$):

$$d_\gamma(a_i, a_j)^2 = \frac{2\pi(i-j)}{N}$$

Rearrangement of F given in (2.3) , shows that the difference in the integrand is governed by just the difference of the squared distances. To this end, we multiply out and using multiple angle formulae we obtain (assuming uniform mesh size)

$$|\gamma(a_i) - \gamma(a_j)|^2 - d_\gamma(a_i, a_j)^2 = 2 - 2\cos\Big(\frac{2\pi(i-j)}{N}\Big) - \frac{4\pi^2(i-j)^2}{N^2}$$

Then recalling i, j are close:

$$\begin{aligned} &= 2 - 2\Big(1 - \frac{2\pi^2(i-j)^2}{N^2} + \frac{2\pi^4(i-j)^4}{3N^4} + \mathcal{O}\Big(\frac{1}{N^6}\Big)\Big) - \frac{4\pi^2(i-j)^2}{N^2} \\ &= -\frac{4\pi^4(i-j)^4}{3N^4} + \mathcal{O}\Big(\frac{1}{N^6}\Big) \end{aligned}$$

As $N \to \infty$, $i-j = \tilde{h} \to 0$ and we have an $\mathcal{O}(\tilde{h}^4)$ rate of convergence of the integrand. From this we may now seek to remove any irregularity in the integrand, so that we may calculate the energy accurately and there are several ways of achieving this.

- Firstly the above calculation shows that the singularity at $F(x, x)$ is a removable singularity in this known fixed curve scenario, and thus one may replace the point $F(x, x)$ with the limit (which is well defined) of $F(x, y)$ as $y \to x$. (in the case of the circle this is the point $F(x, x) = \frac{4\pi^2}{12}$, $\forall\, x$ (this calculation can be found in the appendix). This will be an exact solution.

- Else we can use a smoothing operator (such as the flattening method described in Section 3.2, as F not discretised here one may set $R = 2$ for example) to reduce the error to the order of error to be small.

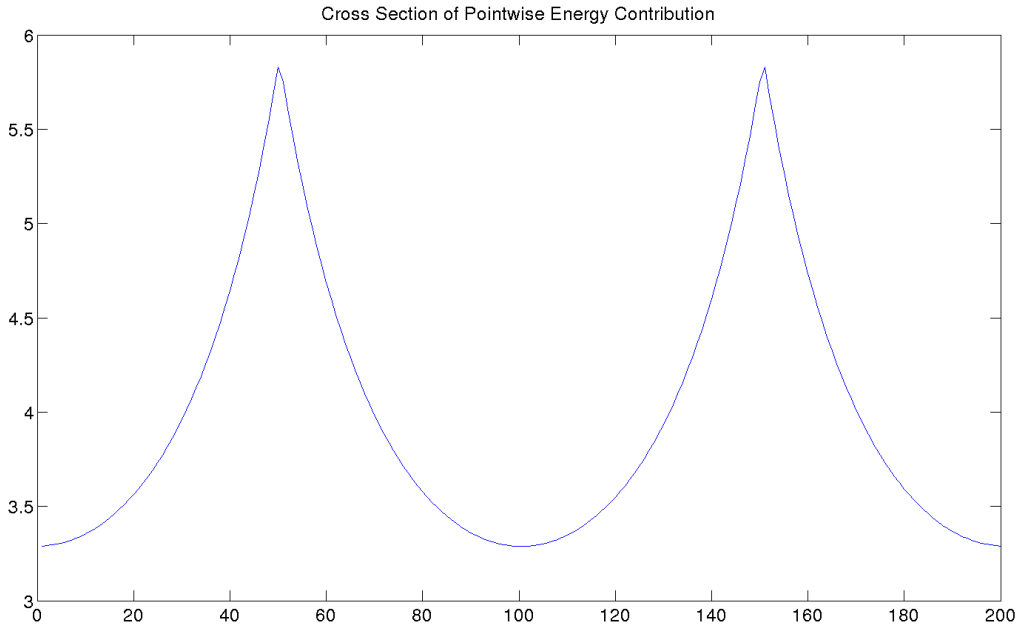

Figure 2.3: *This gives the new cross section with the proposed smoothing (R=2), for a circle with* $N = 200$

Remark. Unfortunately the problem with the cusps cannot be solved so easily. It is easy to construct a counterexample whereby the intersection will occur exactly half-way along the curve. If we cutoff this area therefore we could remove much of the resolution of the self intersection. One could investigate into some smoothing of the cusps however this has not been investigated in detail, as the desired orders of convergence were acheived without this. We can see the improvement in the table below:

Grid size	Error	EOC	Smoothed Error	Smoothed EOC
20	0.2813	–	0.1226	–
40	0.1114	1.4113	0.0310	1.9784
80	0.0475	1.2780	0.0078	1.9932
160	0.0212	1.1663	0.0019	1.9976
320	0.0095	1.0920	0.0005	1.9991
640	0.0040	1.0485	0.0001	1.9996
1280	0.0013	–	0.0000	–

The convergence is clearly improved from order 1 to order 2 by smoothing the curve as in Figure 2.3.

Remark. A note on stability. It is important with the imbalance explored in this subsection to consider possible instabilities of numerics where the Euclidean distance is small, as large numbers are being taken from each other close to the singularity. During testing there was not found any detectable instability for upto $N = 5120$.

2.3 Fixed curve: Discretisation of the integrand

We motivate this section by referencing to the application in later chapters, regarding a time evolution of a closed curve. The question which is asked in application, is not only whether we are able to modify and discretise the integrand fully, perhaps for calculational purposes, but we put more emphasis on whether it is possible for us to calculate a discrete approximate energy accurately without knowing what explicitly Γ is. In other words, if we just have perhaps some form of approximation Γ_N based on N samples of Γ.

The simplest idea for dealing with the integration is to use the *tensor ansatz* again on the double integral and then use quadrature to approximate the integral in each spatial direction using the midpoint rule (Subsection 2.2.1). We approximate the curve Γ by a piecewise linear (constructed from interpolating N points that we use in the quadrature) polynomial $\Gamma_N \in \mathcal{P}_N$ with parametrisation $p_N : [0,1] \to \Gamma_N$ and use the notation $d_N(a_i, a_j)$ for arc length of this approximation between a_i and a_j mesh points in $[0,1]$.

2.3.1 Possibile discretisations

One possible candidate for a discrete energy can be found in the literature, [18]

Definition 2.3.1. *Scholtes's discrete energy* uses an arc-length parametrisation p_N and is given by:

$$E_N(p_N) = \frac{1}{N^2} \sum_{\substack{i \neq j \\ i,j=1}}^{N} \left(\frac{1}{|p_N(a_i) - p_N(a_j)|^2} - \frac{1}{d_N(a_i, a_j)^2} \right) \tag{2.4}$$

This simply ignores diagonal terms and allows the energy summand to be zero here as we initially used in the continuous case. Here however it seems a viable consideration as by the definition of p_N here. if $|a_i - a_j| = \frac{1}{N}$, then then this term equals 0 too.

One important feature of this particular discretisation is that as $N \to \infty$ we have a notion of convergence to our original energy $E(\lim_{N\to\infty} p_N)$, an even stronger result

found in [18] :

Proposition 2.3.1. *Let $q \in [1,2]$, then*

$$E_N \xrightarrow{\Gamma} E \text{ on } (\mathcal{C}, \|\cdot\|_{W^{1,q}([0,1],\mathbb{R}^2)}) \quad \text{as } N \to \infty$$

Where $\mathcal{C}$ is the space of embedded closed curves $\subset \mathbb{R}^2$ with arclength 1.

Remark. Gamma convergence is defined by a "liminf inequality" (for lower semicontinuity) and a "limsup inequality" (for a recovery sequence). That is, to prove the statement above then the two following must be shown:

Let $p_N \in \mathcal{P}_N$ and $p_N \to \gamma$ in $W^{1,1}([0,1],\mathbb{R}^2)$, then

$$E(\gamma) \leq \liminf_{N\to\infty} E_N(p_N)$$

Let $\gamma \in \mathcal{C}$, then there are $p_N \in \mathcal{P}_N$ such that

$$p_N \xrightarrow{W^{1,2}([0,1],\mathbb{R}^2)} \gamma \text{ and } \lim_{N\to\infty} E_N(p_N) = E(\gamma)$$

Here Gamma convergence is with respect to the Sobolev $W^{1,q}$ norm on our domain $[0,1]$, and this type of convergence is specifically designed so that if it holds, minimisers (or almost minimisers) of the energy E_N will also converge to minimisers (or almost minimisers) of E.

It is possible from this result to prove many corollaries as in [18] such as the energy $E_N(p_N)$ for inscibed equilateral polygons p_N will converge (after some rescaling from the unit arclength 1) to $E(\gamma)$. Also we can determine that the unique minimiser of the energy E_N in $\mathcal{P}_N$ is the regular N-gon, which is important for discretisation.

However, the framework in which the Scholtes energy was constructed was intended for the gamma convergence results and other topological uses, for which this energy performs admirably. For our applications we have a few difficulties. The arclength parametrisation disallows the time evolution schemes that we wish to use as it requires full information about the curve for the parametrisation. Also there are problems with the regularity, a lack of smoothness similar to those we found in Subsection 2.2.2 with the continuous problem. This leads to a low convergence rate (Table shows values for the circle):

Grid size	Scholtes's error	Scholtes's EOC
40	0.7712	–
80	0.3677	1.0760
160	0.1763	1.0531
320	0.0841	1.0307
640	0.0389	1.0165
1280	0.0166	1.0085
2560	0.0055	–

Our aim is to come up with a formula for a discrete energy which will improve the convergence and rely less upon the parametrisation as Scholtes's energy.

Definition 2.3.2. the *discrete Möbius energy* is given by:

$$E_N(p_N) = \frac{1}{N^2} \sum_{i,j=1}^{N} \left(\frac{1}{|p_N(a_i) - p_N(a_j)|^2} - \frac{1}{d_N(a_i, a_j)^2} \right) |p'_N(a_i)||p'_N(a_j)| \qquad (2.5)$$

Remark. One should notice we have not specified what value the energy summand F_N will take at (a_i, a_i) - options here will be explored in subsection 2.3.2. Also it should be noticed that this formulation does not depend on information given by γ that will not be resolved by p_N.

Remark. Classically, the derivative of a piecewise linear function is not defined at the interpolating points, we therefore take an average over the derivatives of the coincident linear pieces. This choice is the natural extension from Scholtes's energy to a curve of general arc length.

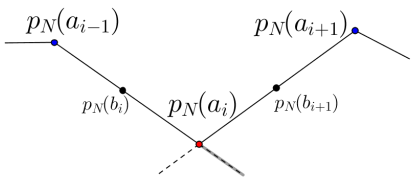

Figure 2.4: *Derivative approximation*

Take a segment of curve, and recall the transformation $(x, y) \mapsto (x + \frac{1}{2}, y + \frac{1}{2})$. If we take the trapezium rule after this transformation of its gridpoints, it is equivalent to performing the midpoint rule on the original gridpoints. On each panel

of the approximation:

$$\int_{b_i}^{b_{i+1}} \int_{b_j}^{b_{j+1}} F(x,y)\,\mathrm{d}y\,\mathrm{d}x \approx \frac{\Big(F(b_i,b_j)+F(b_{i+1},b_j)\Big)+\Big(F(b_i,b_{j+1})+F(b_{i+1},b_{j+1})\Big)}{4N^2}$$

and so, for consistency, we require here to take $p'(b_i) = p'(a_i)^+ \coloneqq \lim_{t\downarrow a_i} p'(t)$, and $p(b_{i+1}) = p'_N(a_{i+1})^- \coloneqq \lim_{t\uparrow a_{i+1}} p'_N(t)$ in the formula for F, as p' is defined at the b_i . Similarly from Figure 2.4 we see you get identically on the segment (a_{i-1}, a_i), thus the combined contributions require

$$p'_N(a_i) \coloneqq \frac{p(a_i)^- + p(a_i)^+}{2} \qquad \forall\, i = 1,\ldots,N$$

2.3.2 Regularity of the integrand

In view of the previous energy possibilities, we wish to improve on the energy (2.4) in terms of convergence, clearly we must modify our energy in order to obtain the regularity that will provide a better order of convergence. To this end we investigate the circle example, and use the new discretisation proposed in Definition 2.3.2. Once again the most clear case of where the integrand F may develop problems with its regularity is where two mesh points are close in terms of the Euclidean distances.

The Euclidean distance between any two grid (for the quadrature and discretisation) points on the circle $a_i = \frac{i}{N}$, $a_j = \frac{j}{N}$ is given by:

$$|p_N(a_i) - p_N(a_j)|^2 = \left(\cos\left(\frac{2\pi i}{N}\right) - \cos\left(\frac{2\pi j}{N}\right)\right)^2 + \left(\sin\left(\frac{2\pi i}{N}\right) - \sin\left(\frac{2\pi j}{N}\right)\right)^2$$

and the discretised arclength is given by (wlog $i > j$):

$$d_N(a_i, a_j) = \sum_{k=j}^{i-1} |p_N(a_{k+1}) - p_N(a_k)|$$

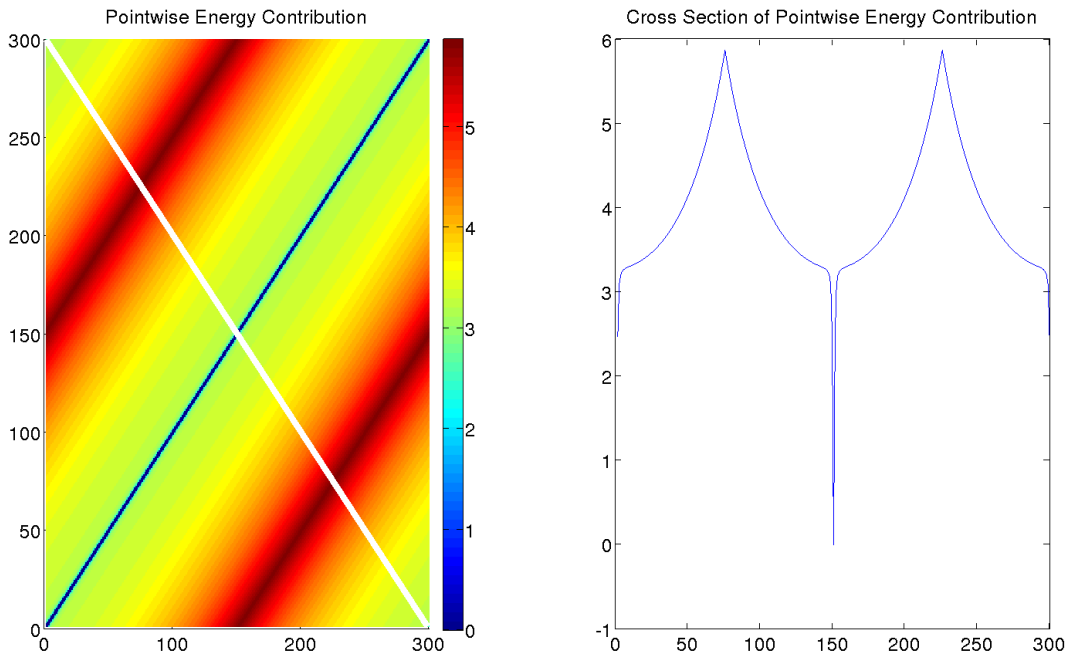

Figure 2.5: *The left: energy density of the approximated unit circle, on the right: the cross section plotted along the white line*

Multiplying out terms we obtain (assuming constant mesh size):

$$
\begin{aligned}
&|p_N(a_i) - p_N(a_j)|^2 - d_N(a_i, a_j)^2 \\
&= 2 - 2\cos\Big(\frac{2\pi(i-j)}{N}\Big) - (i-j)^2\Big(2 - 2\cos\Big(\frac{2\pi}{N}\Big)\Big)^2 \\
&= 2 - 2\cos\Big(\frac{2\pi(i-j)}{N}\Big) - \Big(2(i-j)^2 - 2(i-j)^2\cos\Big(\frac{2\pi}{N}\Big)\Big) \\
&= 2 - 2\Big(1 - \frac{2\pi^2(i-j)^2}{N^2} + \frac{2\pi^4(i-j)^4}{3N^4}\Big) - 2(i-j)^2 + 2(i-j)^2\Big(1 - \frac{2\pi^2}{N^2} + \frac{2\pi^4}{3N^4}\Big) + \mathcal{O}\Big(\frac{1}{N^6}\Big) \\
&= \frac{4\pi^4(i-j)^2(1-(i-j)^2)}{3N^4} + \mathcal{O}\Big(\frac{1}{N^6}\Big)
\end{aligned}
$$

so we see that if $i = j + 1$ we have $\mathcal{O}(h^6)$ error from the Taylor series. Otherwise we have an error term of $\mathcal{O}(h^4)$ for $|i - j| \geq 2$. We look at this behaviour more carefully in the appendix. We also attempt to solve the problem using this analysis in the following chapter.

Chapter 3

Calculation of the discrete Möbius energy

In this chapter we wish to implement the Möbius energy efficently and attempt to obtain convergence rates. For more information regarding the setup and numerical test examples please consult Section 6.3.

One significant implementational issue arises with the discrete Möbius energy. The quantity in which issues originate is the calculation of arc length between any two points on the approximating piecewise linear polynomial curve ∂_N. If there are N data points given on the membrane, then this quantity must be calculated between $\mathcal{O}(N^2)$ points, and the operation itself is $\mathcal{O}(N)$ (one must calculate the distance by 'walking' around the curve length N). Thus the overall computational complexity is $\mathcal{O}(N^3)$.

We propose some solutions to this problem. Firstly we shall consider the actions of a cutoff function, we also propose another possibility of calculation if we may guarantee some form of closeness to equidistribution.

3.1 Linear cutoff function

Recall the formula for our continuous and discrete energy functions:

$$E(\gamma) = \iint_{[0,1]^2} \left(\frac{1}{|\gamma(x) - \gamma(y)|^2} - \frac{1}{d_\gamma(x,y)^2} \right) |\gamma'(x)||\gamma'(y)| \, \mathrm{d}x \, \mathrm{d}y$$

$$E_N(p_N) = \frac{1}{N^2} \sum_{\substack{i \neq j \\ i,j=1}}^{N} \left(\frac{1}{|p_N(a_i) - p_N(a_j)|^2} - \frac{1}{d_N(a_i,a_j)^2} \right) |p'_N(a_i)||p'_N(a_j)|$$

We have chosen to cut 6off the function as a method of reducing the complexity, due to a couple of natural properties of the energy. Firstly the inequality:

$$\forall x, y \in \Gamma \quad d_\gamma(x,y) \geq |\gamma(x) - \gamma(y)| \tag{3.1}$$

this governs the idea of the cutoff function. Imagine the Euclidean distance is relatively large then the geodesic distance will be even larger, and the integrand of the energy will be a difference of two very small objects - thus not contributing to the energy in a significant way. Moreover we are interested in self intersections, thus we are keen to detect phenomena that occur only when Euclidean distances are relatively very small. Another benefit is that not only can the Euclidean distance be efficiently calculated but is needed in the energy itself anyway so we are not required to compute any further quantities. These facts motivate why a cutoff based on the value of the Euclidean distance is a sensible choice. We have chosen a linear cutoff was chosen to avoid a loss of regularity, which as we have seen is an important property to retain.

To this end, let L be the total arclength, then we define the linear cutoff function, using the level sets of the Euclidean distance as a measure. We define some inner cutoff value ($\theta_1 L$ s.t $\theta_1 \in [0,1]$) we calculate the arc length fully; between $\theta_1 L$ and an outer cutoff value ($\theta_2 L$ s.t $\theta_2 \in [\theta_1, 1]$) we contribute only a proportion of the arc distance linearly dependent on the Euclidean distance between points, then by $\theta_2 L$ the energy is 0. Let $t(x,y) = |\gamma(x) - \gamma(y)|$

$$\tilde{d}_\gamma(x,y)^2 = \begin{cases} d_\gamma(x,y)^2 & \text{if } t(x,y) \leq \theta_1 L \\ \frac{1}{(\theta_2 - \theta_1)L}\Big(|\gamma(x) - \gamma(y)|^2 (t(x,y) - \theta_1 L) & \text{if } \theta_1 L < t(x,y) \leq \theta_2 L \\ \qquad + d_\gamma(x,y)^2(\theta_2 L - t(x,y))\Big) & \\ |\gamma(x) - \gamma(y)|^2 & \text{if } t(x,y) > \theta_2 L \end{cases}$$

Definition 3.1.1. The *cutoff Möbius energy functional* as

$$\tilde{E}(\gamma) = \iint_{[0,1]^2} \left(\frac{1}{|\gamma(x) - \gamma(y)|^2} - \frac{1}{\tilde{d}_\gamma(x,y)^2} \right) |\gamma'(x)||\gamma'(y)| \, \mathrm{d}x \, \mathrm{d}y$$

Then discretising as with the original energy with $\tilde{d}_N(\cdot,\cdot)$ analogously defined:

Definition 3.1.2. The *discrete cutoff Möbius energy functional*

$$\tilde{E}_N(p_N) = \frac{1}{N^2} \sum_{\substack{i \neq j \\ i,j=1}}^{N} \left(\frac{1}{|p_N(a_i) - p_N(a_j)|^2} - \frac{1}{\tilde{d}_N(a_i, a_j)^2} \right) |p'_N(a_i)||p'_N(a_j)|$$

Taking a limit as $N \to \infty$ would yield an energy in the continuous setting that is 'equivalent' to the original Möbius energy as firstly $\tilde{E}$ bounds E from below (so a singularity of $\tilde{E}$ is a singularity of the Möbius energy) and also we can find an upper bound as the cutoff is quantifiable due to the inequality $|\gamma(x)-\gamma(y)| > \theta_2 L$ in the definition $\tilde{d}_\gamma(x, y)$ and the bound (3.1). The similar bound $d_N(x, y) \geq |p_N(x) - p_N(y)|$ will show this holds in the discrete case too. One should notice that this discrete cutoff energy will display a lower resolution for phenomena taking place between points greater than $\theta_2 L$ distance apart

Remark. we have chosen a cutoff function with θ_1, θ_2 independent of N. Although this choice seems plausible in the discrete setting, in taking limits one must have convergence of $\{\theta_2(N) \to (\theta > 0)\}$ or $\{\theta_2(N) \to 0\}$. In the first case in numerics we do not observe any real noticeable difference compared to setting $\theta_2 = \theta$. The second case produces a 'delta function' discontinuity at zero, which is troublesome for the convergence analysis and moreover it causes the resolution of the the energy in the discrete setting to become very fine, that is, for larger N the energy spike is sharper and sharper (which if we are considering the extension in Chapter 7 would lead to undesirably sharp behaviour with the forcing term).

Remark. The values of θ_1 and θ_2 are left upto the user, as it is mostly in regards to efficiency. During testing I found with $N > 200$ points you may θ_1 as low as 0.05 or so and still acheived accurate sharp peaks. One must be careful that this cutoff is large enough to not interfere with the smoothing described in the next chapter.

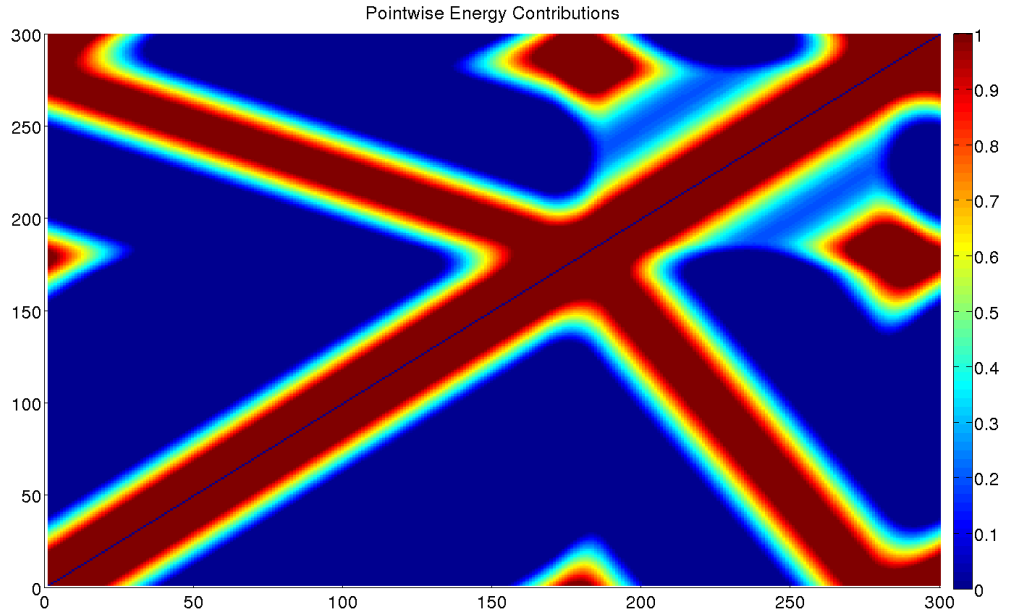

Figure 3.1: $\theta_1 = 0.06$, $\theta_2 = 0.12$ $N = 300$ *on a C-shape membrane (see Section 6.3), the value 1 indicates* $\tilde{d}_\gamma = d_\gamma$*, the value 0 indicates the* $\tilde{E}_N = 0$.

From the parametrisation of this shape (given in the appendix), we can describe the behaviour of Figure 3.1. The red strip along the diagonal represents neighbouring points in the parametrisation (and so are naturally close in Euclidean distance) are taken into account. The red path that crosses the diagonal represents that for each point on the inner part of the membrane, the closest points on the outer part of the membrane are taken into account. The two red diamonds represent the ends of the C-shape being close. Recalling the periodicity takes into account the other behaviour.

3.2 Smoothing the integrand

We wish to avoid also the problematic areas where the geodesic (and by (3.1), Euclidean) distances tend to be very small. These lead to the difference in the integrand becoming very large and so may cause instability. We have seen that if one implemented the continuous integrand on for example the circle then one would just have to set the singular value for points $F(\gamma(a_i), \gamma(a_j))$ where $i = j$ equal to value at $F(\gamma(a_{i+1}), \gamma(a_i))$. This is because we know from Subsection 2.2.2, that the singularity is only at 0, and also the convergence is very rapid, so there is little error

in this change.

However, in the discrete integrand case we have two further problems. Our linear polynomial approximation p_N leads to the Euclidean distance and discrete geodesic distances coincide for neighbouring gridpoints - so setting our values $F(\gamma(a_i), \gamma(a_i)) = F(\gamma(a_{i+1}), \gamma(a_i))$ will not alter the behaviour of the integrand therefore we must alter these values further from the core of the instability.

3.2.1 Flattening method

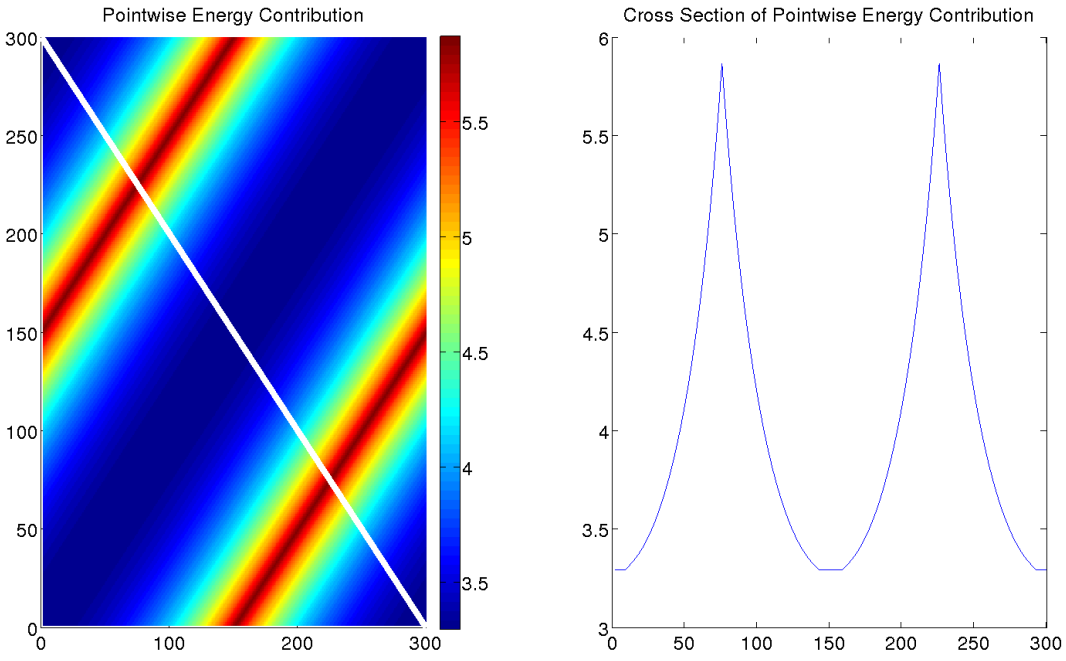

Figure 3.2: *The left: smoothed energy density of estimated unit circle, on the right: the cross section plotted along the white line (see Figure 2.5 for unsmooth case)*

The smoothing function can vary, however we pose a couple in this paper, the first I have called 'the flattening method'. It takes a radius $R \in \{1, \ldots, \lfloor \frac{N}{2} \rfloor\}$ and there are $a_{R^-}, a_{R^+} \in \{x : |\gamma(a_i) - \gamma(x)| = R\}$ then set

$$F(\gamma(x), \gamma(a_i)) = F(\gamma(a_{R^+}), \gamma(a_i)), \qquad \forall\, x \in \{-a_{R^-+1}, \ldots, a_{R^+-1}\} \tag{3.2}$$

This leads to the creation of the smoothed energy profiles seen in Figure 3.2

Remark. The choice of the radius R can be made in many ways, but it can be an im-

portant factor in determining the convergence, thus a sensible choice must be made. For a fixed point x on Γ as we have seen the energy integrand is an approximation of a inverted-quadratic-like function (See the appendix for the derivation)

$$F_x(y) = \begin{cases} \alpha(1 - \frac{1}{(y-(x-h))^2}) & y < x - h \\ 0 & x - h \leq y \leq x + h \\ \alpha(1 - \frac{1}{(y-(x+h))^2}) & y > x + h \end{cases}$$

where, for example the unit circle $\alpha = \frac{\pi^2}{3}$. Near the instability we are interested on fixing a value of F as in (3.2), thus one would invert this relation to observe the behaviour of the region of influence. i.e let $\tilde{x} = y - (x + h)$ then for the $y > (x + h)$ branch:

$$\tilde{x} = \sqrt{\frac{1}{1 - \frac{3}{\pi^2}F}}$$

Thus if we wished to fix a value of such as $F_x(y) = \frac{\pi^2}{3} - \frac{1}{N}$ (which seems a sensible choice as it will converge to the value of the limiting value at x as $N \to \infty$), we would require the radius of the cutoff to be:

$$R = \sqrt{\frac{1}{1 - \frac{3}{\pi^2}(\frac{\pi^2}{3} - \frac{1}{N})}} = \sqrt{\frac{\pi^2}{3}N} = C\sqrt{N}$$

Which indicates that we would wish the radius to be of order $\sqrt{N}$. This is promising as it means that the section of the curve that is smoothed will shrink to 0 as $N \to \infty$.

The constant α, on a general surface will be a function $\alpha(x)$ of the curvature $\kappa(x)$ at x, motivating my choice of radius here (to construct Figure 3.2)

$$R = \frac{1}{\tilde{\kappa}}N^{\frac{1}{2}} \qquad \text{where } \tilde{\kappa} = \max_{i=1,\ldots,N} \kappa(a_i)$$

3.2.2 A smoothing cutoff function

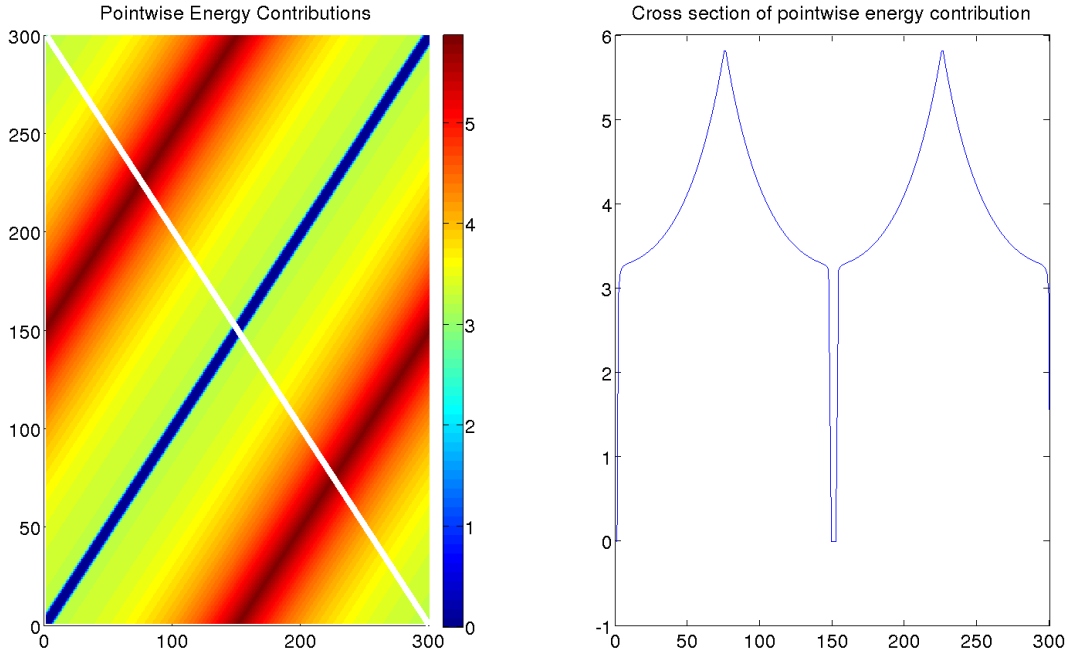

Figure 3.3: *The left: smoothed energy density of estimated unit circle, on the right: the cross section plotted along the white line (see Figure 2.5 for unsmooth case)*

Another alternative is to use another cutoff function but instead of for the purpose of efficiency we use a quadratic smoothing to improve the regularity. One simply has to use a function whose value is zero around the singularity and one at prescribed radius about the singularity, and also to keep the regularity one must ensure the derivatives vanish at the endpoints of the interval. We opt to use to cutoff values ψ_1, ψ_2 and as in the linear case, these are fixed as a proportion of the total (approximate) arclength of the curve.

Then we use the smoothing function which is based on the cubic polynomial $t^2(3-2t)$. Let $t(x,y) = |p_N(x) - p_N(y)|$:

$$\tilde{d}_\gamma(a_i,a_j)^2 = \begin{cases} |p_N(a_i)-p_N(a_j)|^2 & \text{if } t(a_i,a_j) < \psi_1 L \\ |p_N(a_i)-p_N(a_j)|^2 + \left(\frac{t(a_i,a_j)-\psi_1}{(\psi_2-\psi_1)L}\right)^2 \left(3-2\frac{t(a_i,a_j)-\psi_1}{(\psi_2-\psi_1)L}\right) & \text{if } \psi_1 L \le t(a_i,a_j) < \psi_2 L \\ \qquad \cdot\left(d_N(a_i,a_j)^2 - |p_N(a_i)-p_N(a_j)|^2\right) & \\ d_N(a_i,a_j)^2 & \text{if } \psi_2 L \le t(a_i,a_j) \end{cases}$$

Remark. We could use a similar quadratic for the efficiency cutoff above but no noticeable difference was seen in the convergence, however I did not see a significant difference compared to added computational costs.

3.3 Equidistribution method

Another possibility which can be implemented in the discrete setting and without the need of a cutoff function is to get efficiently computable upper and lower bounds on the energy. Given N data points on the membrane so in the discrete setting we are working on a linear interpolation of the membrane between these N points. Recall that $d_N(a_i, a_j)$ (wlog $i < j$) is therefore a sum of the lengths of neighbouring edges $\sum_{k=i+1}^{j} |\gamma(a_k) - \gamma(a_{k-1})|$. So we can obtain bounds on the arc lengths on the interpolated curve Γ_h by finding the minimum and maximum edge lengths:

$$\text{let } q_{\min} \text{ be such that } q_{\min} = \min_{i=1,\dots,N} |\gamma(a_i) - \gamma(a_{i-1})|$$
$$\text{let } q_{\max} \text{ be such that } q_{\max} = \max_{i=1,\dots,N} |\gamma(a_i) - \gamma(a_{i-1})|$$

(indices modulo N)then define the minimal and maximal total arclength of Γ_h by $L_{\min} = Nq_{\min}$, $L_{\max} = Nq_{\max}$. Finally we may define the new geodesic distances by

$$\tilde{d}_{\min,N}(a_i, a_j) = \min\{(j-i)q_{\min}\ ,\ L_{\min} - (j-i)q_{\min}\}$$
$$\tilde{d}_{\max,N}(a_i, a_j) = \max\{(j-i)q_{\max}\ ,\ L_{\max} - (j-i)q_{\max}\}$$

This operation is now $\mathcal{O}(1)$ so reduces the overall complexity to $\mathcal{O}(N^2)$ of the calculation. However we must be able to control the deviation of $q_{\min}$ from $q_{\max}$, as clearly we observe that the error in this approximation increases significantly if the ratio $\frac{q_{\max}}{q_{\min}} \gg 1$.

To obtain control of this ratio, one could use the BGN method for the surface evolution as a remeshing step, this is possible as it contains the tangential equidistribution motion across the membrane. One simply must condition on performing timestep only if for example the ratio $1 \leq \frac{q_{\max}}{q_{\min}} < 1.3$, then if this condition is not satisfied you use the BGN with a very small timestep $\tilde{\tau} = \tau^2$ or τ^3 to remesh until the ratio is satisfied.

3.4 Numerics for fixed curve

Please consult Section 6.3 for details on the testing setup.

Shapes: (A) circle, (B) ellipse, (C) C-shape

3.4.1 EOC for the discrete energy

The following table displays the original generalisation of Scholtes's energy (2.4) to for curves of arbitrary arclength. That is, the energy

$$E_N(p_N) = \frac{1}{N^2} \sum_{\substack{i \neq j \\ i,j=1}}^{N} \left(\frac{1}{|p_N(a_i) - p_N(a_j)|^2} - \frac{1}{d_N(a_i, a_j)^2} \right) |p'_N(a_i)||p'_N(a_j)|$$

Grid size	A error	A EOC	B error	B EOC	C error	C EOC
20	0.6904	–	1.1382	–	20.6350	–
40	0.3453	0.9812	0.5289	1.1431	7.5140	1.4183
80	0.1704	0.9927	0.2531	1.0631	2.6047	1.6755
160	0.0826	0.9969	0.1211	1.0257	1.0678	1.3287
320	0.0386	0.9986	0.0562	1.0108	0.4560	1.1806
640	0.0165	0.9993	0.0240	1.0048	0.1860	1.1051
1280	0.0055	–	0.0080	–	0.0605	–

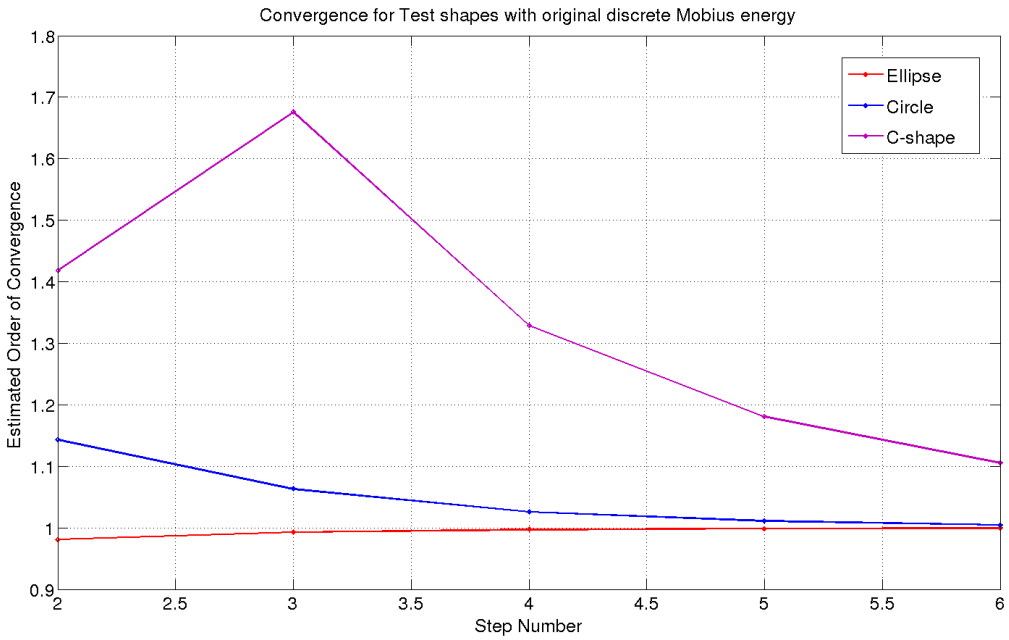

Figure 3.4: *Graph of the above table for our original discrete Möbius energy*

As you can see the convergence for all shapes is of order 1. So we have not yet improved upon the convergence that the original energy had, although generalisation has not decreased the orders convergence either.

Aside from obtaining convergence rates, the central purpose of this energy is to actually detect curve intersections. The graphs on the following page demonstrate this for one of the test shapes for $N = 200$. There is a definite spike even with a relatively low N, with almost 4 times the energy at intersection, also one can see this energy density is entirely concentrated with small support around the the tips with spikes of height $1,800,000$. This reinforces that if we implemented a cutoff function outside these areas should not affect the energy value significantly.

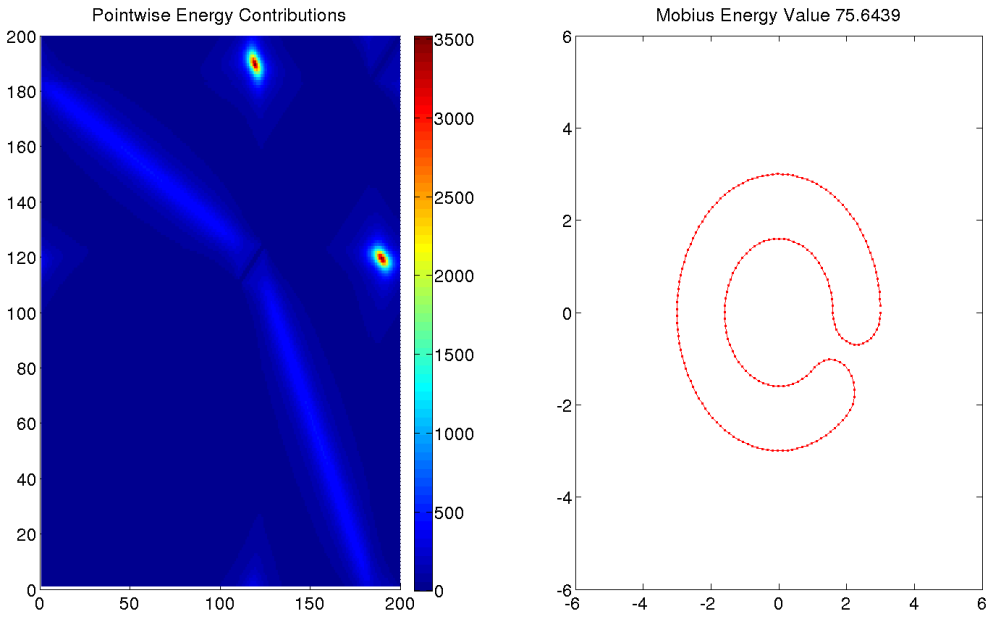

Figure 3.5: *Energy integrand density. Total Möbius energy = 75.6439*

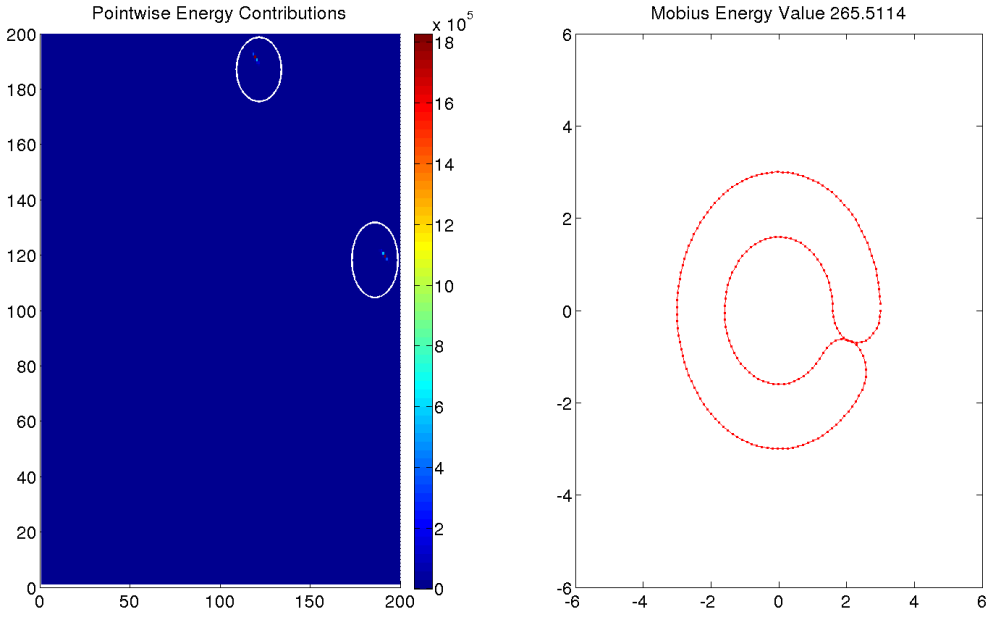

Figure 3.6: *Energy integrand density. White circles indicate the position of the energy spikes. Total Möbius energy = 265.5114*

3.4.2 EOC for the discrete cutoff Möbius energy

We now show some EOC tables for the energy with varying cutoff values θ_1, θ_2, the numbers represented below give the value of θ_1, and we set $t_2 = 1.1\theta_1$.

Grid size	0.3 error	0.3 EOC	0.2 error	0.2 EOC	0.1 error	0.1 EOC
20	29.6968	–	29.8614	–	26.0196	–
40	12.2574	1.0582	12.2682	1.0688	11.5349	0.8665
80	3.8826	1.7542	3.8811	1.7562	3.5905	1.8243
160	1.4000	1.5314	1.3982	1.5315	1.3472	1.4497
320	0.5411	1.3690	0.5394	1.3730	0.5259	1.3484
640	0.2086	1.2113	0.2078	1.2127	0.2034	1.2120
1280	0.0650	–	0.0647	–	0.0642	–

Grid size	0.05 error	0.05 EOC
40	6.9325	–
80	2.8303	1.3525
160	1.2239	1.2104
320	0.5297	1.1989
640	0.2273	1.1405
1280	0.0902	1.1981
2560	0.0304	–

We still appear to get convergence to order 1 as with the original energy. We note that the increasing cutoff although asymptotically will not affect the limit of 1, (as one expects because it does not bottleneck more than the regularity issues), it does appear to reduce the actual values attained. The more of the curve is cutoff the lower the convergence order - which may cause practicality issues with actual error values.

I believe the computational benefits far outweigh this slight reduction in convergence, as you are capable of performing more EOC steps as general calculations are upto about 10 times faster and thus more accuracy can be with a smaller θ_1, θ_2 due to the increase in mesh points available. To see the effects on the energy peak one can see the numerics in Section 6.3.4.

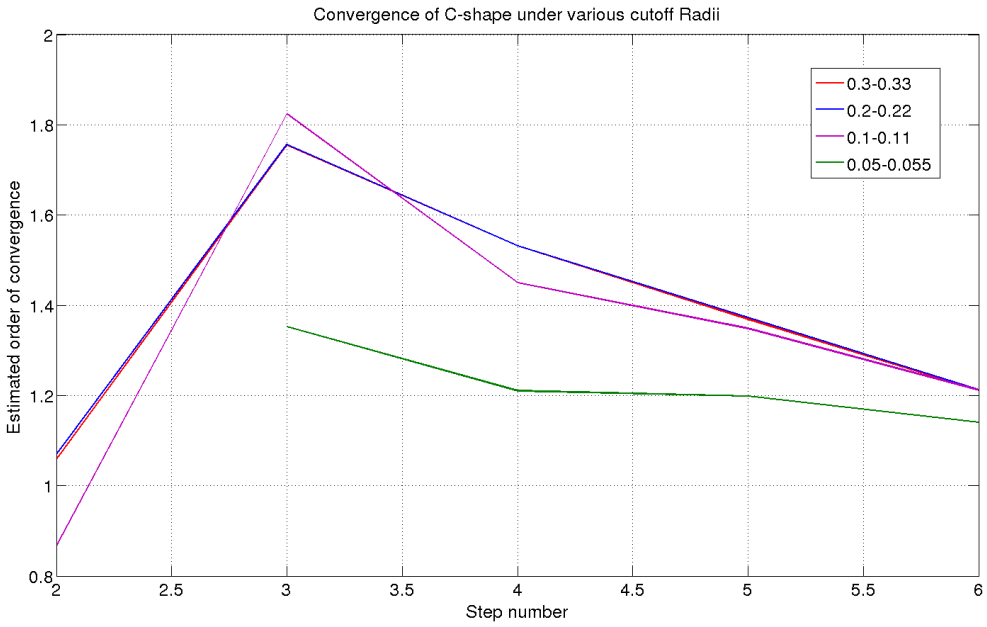

Figure 3.7: *Cutoff values ($\theta_1 = 0.05$ too small for size 20 - no data for this step)*

3.4.3 EOC of the discrete Möbius energy with smoothing

Finally we display the convergence rates using the smoothed discrete energy from Section 3.2

Grid size	A error	A EOC	B error	B EOC	C error	C EOC
20	0.2779	–	0.2563	–	23.7102	–
40	0.0714	2.1045	0.1808	-0.2613	9.6285	0.9348
80	0.0234	1.4712	0.0903	0.9347	2.2622	2.1641
160	0.0060	2.0298	0.0429	0.7769	0.6185	1.8521
320	0.0018	1.6463	0.0153	1.2780	0.1633	1.9884
640	0.0004	2.0522	0.0039	1.9867	0.0485	1.6789
1280	0.0001	–	0.0010	–	0.0127	–

This regularistion appears to cause the convergence to increase to 2 as predicted. An open question arises which is to attempt to generalise the results of [11] and [12] to many dimensions. Certainly with our ansatz and periodicity one could predict our findings.

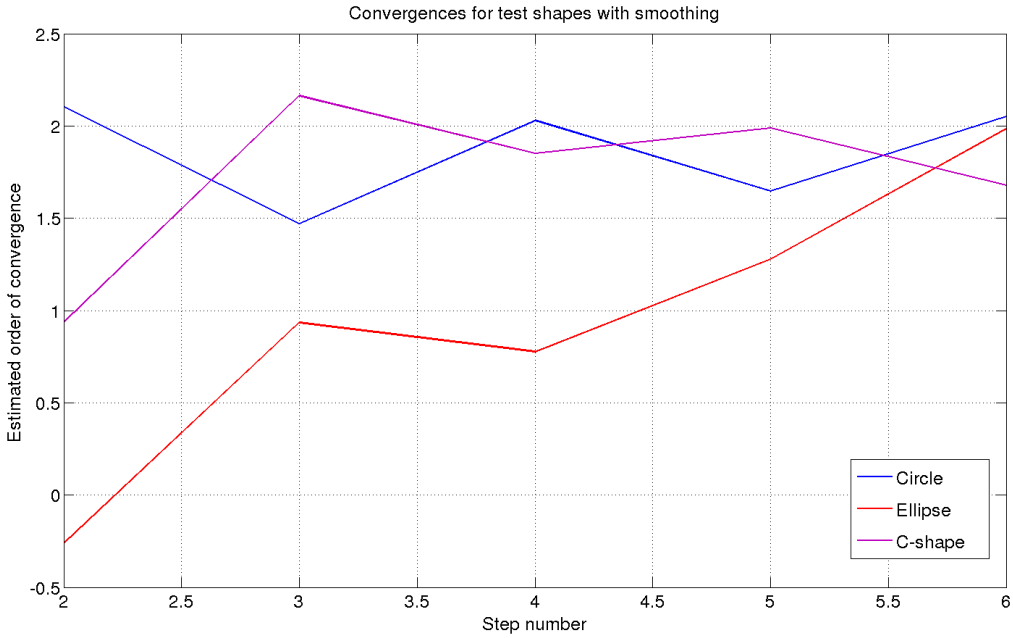

Figure 3.8: *Graph of the above table with the smoothed curves, flattening approach*

We now use the method of a smooth cutoff function to smooth the curve at the irregularities with values that scale with N, in this case we have taken $\psi_1 = \frac{N}{80}$ and $\psi_2 = \frac{N}{40}$.

Grid size	A error	A EOC	B error	B EOC	C error	C EOC
20	0.8747	–	1.3590	–	30.5559	–
40	0.3679	1.0296	0.5496	1.1321	12.1853	1.0425
80	0.1197	1.2556	0.1802	1.2673	3.2665	1.7874
160	0.0157	3.1423	0.0268	2.9470	0.6829	2.3336
320	0.0039	1.9757	0.0069	1.9430	0.1703	2.0318
640	0.0009	1.9834	0.0017	1.9454	0.0450	1.7777
1280	0.0002	–	0.0004	–	0.0084	–

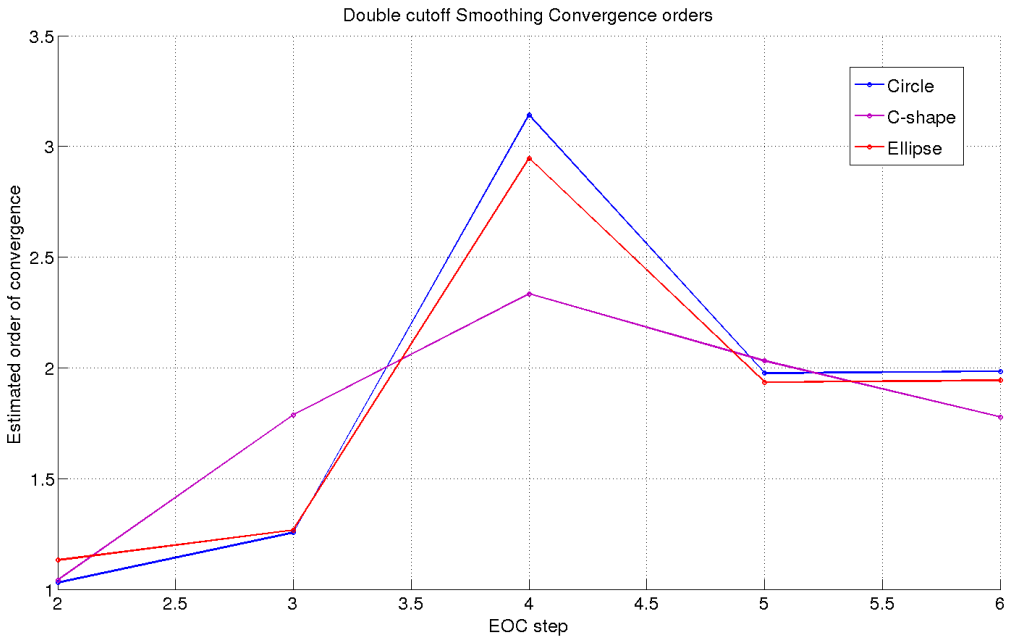

Figure 3.9: *Graph of the above table with the smoothed curves double cutoff approach*

Chapter 4

Surface PDE model for quantities on the membrane

4.1 Derivation

We now proceed with the model of the membrane, which is acheived with an evolving hypersurface $\Gamma = \{\Gamma(t)\}_t$ with given material velocity $v\colon (0,T) \times \Gamma \to \mathbb{R}^2$, where $\mathcal{G} = \{(t, \Gamma(t)) | t \in [0,T]\}$

The *material derivative* is denoted $\partial_t^\bullet f \coloneqq \partial_t f + v \cdot \nabla_f$ and is in some sense the correct time derivative (to be seen later) when dealing with quantities that evolve over time on a moving body.

Now first we let $u\colon \Gamma \to \mathbb{R}$ denote a density on a surface of a conserved quantity. Neglecting reactions with any other species, the postulate a diffusion with tangential flux $q(t) = -D\nabla_{\Gamma(t)} u(t)$, ($D$ constant), and assume there is a source term $f\colon \Gamma \to \mathbb{R}$ of this quantity. With $G \subset \Gamma$ with smooth boundary and unit conormal $\boldsymbol{\mu}$, we may write the balance of mass equations:

$$\underbrace{\frac{\mathrm{d}}{\mathrm{d}t} \int_{G(\cdot)} u(\cdot, x)\, \mathrm{d}\mathcal{H}^{n-1}(x)\Big|_t}_{\text{Mass change in G}} = \underbrace{-\int_{\partial G(t)} q(t,x) \cdot \boldsymbol{\mu}(t.x)\, \mathrm{d}\mathcal{H}^{n-2}(x)}_{\text{net flux over } \partial G} + \underbrace{\int_{G(t)} f(t,x)\, \mathrm{d}\mathcal{H}^{n-1}(x)}_{\text{source of } u} \tag{4.1}$$

From this we may construct the strong form of the surface PDE, as the above holds $\forall G \subset \Gamma$. We obtain a *Divergence Theorem* type result for the surfaces.

$$\int_{\Gamma(t)} \nabla_{\Gamma(t)} \cdot v\, \mathrm{d}\mathcal{H}^{n-1} = -\int_{\Gamma(t)} v \cdot \boldsymbol{\kappa}\, \mathrm{d}\mathcal{H}^{n-1} + \int_{\partial\Gamma(t)} v \cdot \boldsymbol{\mu}\, \mathrm{d}\mathcal{H}^{n-2}$$

The derivation of this can be found in the Appendix.

We may now derive the strong form of the surface PDE, using (4.1) and the divergence theorem derived yield:

$$-\int_{\partial G} q\cdot\boldsymbol{\mu}\,\mathrm{d}\mathcal{H}^{n-2} = -\int_{\partial G} D\nabla_{\Gamma(t)}u\cdot\boldsymbol{\mu}\,\mathrm{d}\mathcal{H}^{n-2} = -\underbrace{\int_G D\nabla_{\Gamma(t)}u\cdot\boldsymbol{\kappa}\,\mathrm{d}\mathcal{H}^{n-1}}_{=0\text{ (tangential flow)}} - \int_G D\Delta_{\Gamma(t)}u\,\mathrm{d}\mathcal{H}^{n-1}$$

Using the transport identity (9.2) we obtain,

$$\frac{\mathrm{d}}{\mathrm{d}t}\int_G u(\cdot,x)\,\mathrm{d}\mathcal{H}^{n-1}\Big|_t = \int_G (\partial_t^\bullet u + u\nabla_{\Gamma(t)}\cdot v)\,\mathrm{d}\mathcal{H}^{n-1},$$

so substitute all into (4.1)

$$\int_G (\partial_t^\bullet u + u\nabla_{\Gamma(t)}\cdot v)\,\mathrm{d}\mathcal{H}^{n-1} = -\int_G D\Delta_{\Gamma(t)}u\,\mathrm{d}\mathcal{H}^{n-1} + \int_G f\,\mathrm{d}\mathcal{H}^{n-1}$$

as G is arbitrary, we can remove the integrals to obtain the strong form of our problem:

Problem 4.1.1. *For $v:\mathcal{G}\to\mathbb{R}^2$, $f:\mathcal{G}\to\mathbb{R}$ given, find $u\in C^2(\mathcal{G})$ such that*

$$\partial_t^\bullet u + u\nabla_{\Gamma(t)}\cdot v - D\Delta_{\Gamma(t)}u = f \quad \text{ on } \Gamma(t)$$

with $u(x,0)=u_0(x)\in C^2(\Gamma(0))$ and we impose the Neumann boundary conditions $q(t)\cdot\boldsymbol{\mu}(t)=g(t)$ at $\partial\Gamma(t)$ where $g\colon\{(t,\partial\Gamma(t))|t\in[0,T]\}\to\mathbb{R}$

4.2 Weak form

(For the sake of bevity we now drop the t in $\nabla_{\Gamma(t)}$ and $\Gamma(t)$.) The derivation of this weak form can be found in the Appendix. Our weak problem can now be stated (using the notation of $L^p(a,b;V)$ to denote the Bochner space on $[a,b]$ and V)

Problem 4.2.1. *for $f\in L^2(\Gamma)$, $g\in L^2(\partial\Gamma)$ and v given, find $u\in L^2(0,T;H^1(\Gamma))$ such that for all test functions $\phi\in L^2(0,T;H^1(\Gamma))$*

$$\frac{d}{dt}\Big(\int_{\Gamma(\cdot)} u\varphi\,d\mathcal{H}^{n-1}\Big)\Big|_t + \int_\Gamma -u\partial_t^\bullet\varphi + D\nabla_\Gamma u\cdot\nabla_\Gamma\varphi\,d\mathcal{H}^{n-1} = \int_\Gamma f\varphi\,d\mathcal{H}^{n-1} - \int_{\partial\Gamma} g\varphi\,d\mathcal{H}^{n-2} \tag{4.2}$$

with $u(x,0)=u_0(x)\forall\, x\in H^1(\Gamma(0))$, and Neumann boundary $q(t)\cdot\boldsymbol{\mu}(t)=g(t)$ on $\partial\Gamma(t)$

Proposition 4.2.1. *[6] Well posedness of and energy estimates of* (4.2)

4.3 Discretisation with ESFEM

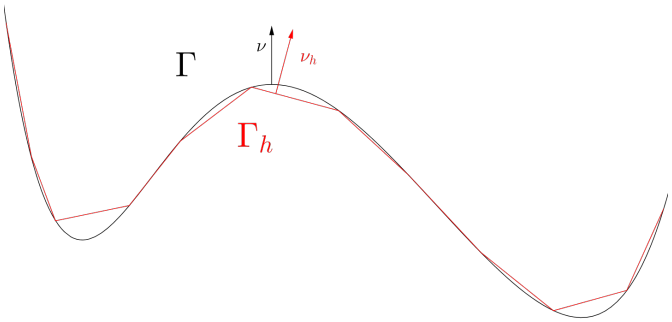

Figure 4.1: *Example of membrane discretisation*

Setting up the evolving surface finite element scheme for this system requires a finite element space and basis functions on our curve $\Gamma(\cdot)$. To this end we consider the discretisation of $\Gamma(t)$ into $\Gamma_h(t)$ set up in Section 2.3, where $h = \frac{1}{N}$ (see Figure 4.1) for each t, and wish to consider isoparametric linear finite elements (the local to global mapping will be piecewise affine). It is now possible to define the space

$$S_h(t) \coloneqq \{f \in C^0(\Gamma_h(t)) \big| \quad f|_T \text{ affine linear polynomial on } T \in \Gamma_h(t)\}$$

and $\{b_i(\cdot,t),\ i \in \mathcal{I}\}$ the corresponding basis functions for $S_h(t)$: let $\{x_i(t)\}_{i=1}^N$ be the mesh point coordinates on $\Gamma_h(t)$, then $b_i(x_j(t),t) = \delta_{ij}$.
We have written the *Continuous problem* and for the closed curve problem we get (4.2) with $g = 0$.

For ease of notation, let $\mathcal{G}_h = \{(t, x_h) | \, x_h \in \Gamma_h(t), t \in [0,T]\}$. Also we define the lift f_h as the discretisation and projection of f onto Γ_h, We can then define the *Semi-discrete problem*, by this discretisation in space.

Problem 4.3.1. *Find* $u_h : \mathcal{G}_h \to \mathbb{R}$ *with* $u \in S_h(t)\, \forall t \in [0,T]$ *with initial data* $u_h(x,0) = u_0(x)$ *on* $\Gamma_h(0)$, *and* $\varphi_h : \Gamma_h \to \mathbb{R}$ *(test function):*

$$\int_{\Gamma_h} f_h\varphi_h \, d\mathcal{H}^{n-1} = \frac{d}{dt}\left(\int_{\Gamma_h(\cdot)} u_h\varphi_h \, d\mathcal{H}^{n-1}\right)\Big|_t + \int_{\Gamma_h} -u_h\partial_t^{\bullet(v_h)}\varphi_h + D\nabla_{\Gamma_h}u_h\cdot\nabla_{\Gamma_h}\varphi_h \, d\mathcal{H}^{n-1} \tag{4.3}$$

We use the discretised material derivative $\partial_t^{\bullet(v_h)}u_h \coloneqq \partial_t u_h + v_h \cdot \nabla u_h$. An important property of this quantity is that the information it contains is completely

contained in the basis functions of the elements, i.e we have the identity $\partial_t^{\bullet(v_h)} b_i = 0$ for all $i \in \mathcal{I}$. The notation f_h and u_{0h} are any appropriate discretisations.

Definition 4.3.1. The *Mass matrix* $\{M_{ij}\}_{i,j\in\mathcal{I}}$ and *Stiffness matrix* $\{S_{ij}\}_{i,j\in\mathcal{I}}$ are the following matrices:

$$M_{ij}(t) \coloneqq \int_{\Gamma_h} b_i(x,t) b_j(x,t) \,\mathrm{d}\mathcal{H}^{n-1} \text{ and } S_{ij}(t) \coloneqq \int_{\Gamma_h} \nabla_{\Gamma_h} b_i(x,t) \cdot \nabla_{\Gamma_h} b_j(x,t) \,\mathrm{d}\mathcal{H}^{n-1}$$

We represent our solution with the Galerkin approximation $u_h(t,x) = \sum_{i\in\mathcal{I}} u_i(t) b_i(x,t)$, and substitute in (4.3), and for each $j \in \mathcal{I}$ use test function $\varphi = b_j$, the basis functions.

$$\int_{\Gamma_h} f_h b_j \,\mathrm{d}\mathcal{H}^{n-1} = \frac{\mathrm{d}}{\mathrm{d}t} \Big(\int_{\Gamma_h(\cdot)} u_h b_j \,\mathrm{d}\mathcal{H}^{n-1} \Big)\Big|_t + \int_{\Gamma_h} -u_h \underbrace{\partial_t^{\bullet(v_h)} b_j}_{=0} + D \nabla_{\Gamma_h} u_h \cdot \nabla_{\Gamma_h} b_j \,\mathrm{d}\mathcal{H}^{n-1}$$

$$\sum_{i\in\mathcal{I}} f_i(t) \int_{\Gamma_h} b_i b_j \,\mathrm{d}\mathcal{H}^{n-1} = \frac{\mathrm{d}}{\mathrm{d}t} \Big(\sum_{i\in\mathcal{I}} u_i(\cdot) \int_{\Gamma_h(\cdot)} b_i b_j \,\mathrm{d}\mathcal{H}^{n-1} \Big)\Big|_t + D \sum_{i\in\mathcal{I}} u_i(t) \int_{\Gamma_h} \nabla_{\Gamma_h} b_i \cdot \nabla_{\Gamma_h} b_j \,\mathrm{d}\mathcal{H}^{n-1}$$

Now we may write this in terms of our mass and stiffness matrices.

$$\sum_{i\in\mathcal{I}} f_i(t) M_{ij}(t) = \frac{\mathrm{d}}{\mathrm{d}t} \Big(\sum_{i\in\mathcal{I}} u_i(\cdot) M_{ij}(\cdot) \Big)\Big|_t + D \sum_{i\in\mathcal{I}} u_i(t) S_{ij}(t)$$

$$M(t) f(t) = \frac{\mathrm{d}}{\mathrm{d}t} \Big(M(\cdot) u(\cdot) \Big)\Big|_t + D S(t) u(t)$$

To fully discretise the scheme we employ the backwards Euler scheme (a fully implicit scheme):

Problem 4.3.2. *Given initial data u^0, timestep τ, solve for $n = 0, 1, 2, 3, ...$*

$$\frac{M^{n+1}u^{n+1} - M^n u^n}{\tau} + S^{n+1} u^{n+1} = M^{n+1} f^{n+1}$$

$$\implies \Big(\frac{1}{\tau} M^{n+1} + S^{n+1} \Big) u^{n+1} = \frac{1}{\tau} M^n u^n + M^{n+1} f^{n+1} \tag{4.4}$$

4.4 Discretisation with ALE ESFEM

The above evolving surface finite element method does have a restriction, which when combined with certain schemes such as 5.2 may lead to inaccuracy. That is, it is constructed such that the meshpoints of the grid we have created, is assumed to move *only* respect to the material velocity (previously denoted v). The Barrett-Garcke Nürnberg scheme referenced in 5.2 will move the meshpoints in the normal direction as in accordance with material velocity but also introduces some surface curvature flow in the tangential direction, which (as it is constructed within the scheme) will be unrelated to the material body motion.

If this is not taken into account then we could have serious accuracy problems, which is fundementally based on the idea of mass conservation and transfer over the surface. If points in the mesh are moved in a different manner to that which is perceived by the finite elements, we will assign mass to a point x say, when actually it is assigned to $\tilde{x}$, then the difference $x \to \tilde{x}$ should cause mass flux in (4.1) to be altered (but it is not).

We have chosen to use a similar scheme created in [9] known as ALE ESFEM. The key idea of this finite element method is to weaken the dependancy of the meshpoints on the material body, so as to allow arbitrary tangential flow of points along a body. The cost of this weakening is that one has to include another matrix in the discretisation to keep track of how exactly the mass change is affected by the new arbitrary movement.

We decompose the material velocity into tangential and normal components: $v := v_\tau + v_\nu$. Consider the velocity of our mesh grid to be of the form (depending on h) $w := v_\nu + w_\tau$ where $w_\tau \cdot \nu = 0$, but $w_\tau \neq v_\tau$.

We use the same finite element space as in the previous method, recall the definition: $S_h(t) := \{f \in C^0(\Gamma_h(t)) \big| \quad f|_T \text{ affine linear polynomial on } T \in \Gamma_h(t)\}$ and $\{b_i(\cdot,t),\ i \in \mathcal{I}\}$ the corresponding basis functions for $S_h(t)$.

Definition 4.4.1. for mesh points $\{x_i(t)\}_{i\in\mathcal{I}}$ on $\Gamma_h(t)$, material velocity v, define the *mesh material velocity* and the *interpolated material velocity* by

$$w_h(x,t) = \sum_{j\in\mathcal{I}} \partial_t x_j(t) b_j(x,t) \quad \text{and} \quad v_h(x,t) = \sum_{j\in\mathcal{I}} v(x_j(t),t) b_j(x,t)$$

and recall the associated material derivatives:

$$\partial_t^{\bullet(w_h)} f := \partial_t f + w_h \cdot \nabla f \quad \text{and} \quad \partial_t^{\bullet(v_h)} f := \partial_t f + v_h \cdot \nabla f$$

Remark. In the section 4.3 it is assumed that we have $\partial_t(x_i(t)) = v_h(x_j(t), t)$, leading to $w_h = v_h$ above, and from there we could obtain the transport identity $\partial_t^{\bullet(v_h)} b_i = 0$, $\forall i$ for the basis functions. Here we actually have $\partial_t(x_i(t)) = w_h(x_j(t), t)$, and we obtain the transport identity (by definition) $\partial_t^{\bullet(w_h)} b_i = 0$, $\forall i$. This leads (via the definition of material derivative) to $\partial_t b_i = -w_h \cdot \nabla b_i$. So we also obtain the identity

$$\partial_t^{\bullet(v_h)} b_i = (v_h - w_h) \cdot \nabla b_i \quad \forall\, i \in \mathcal{I} \tag{4.5}$$

Consider once again the discretised weak formulation of our surface PDE (4.3), and for $j \in \mathcal{I}$ let the test functions $\varphi_h \in H^1(\Gamma_h(t))$, be given by the basis functions $\varphi_h(\cdot) = b_j(\cdot, t)$. Then we use identity (4.5)

$$\int_{\Gamma_h} f_h b_j \,\mathrm{d}\mathcal{H}^{n-1} = \frac{\mathrm{d}}{\mathrm{d}t}\Big(\int_{\Gamma_h} u_h b_j \,\mathrm{d}\mathcal{H}^{n-1}\Big) + \int_{\Gamma_h} u_h (w_h - v_h)\cdot\nabla b_j + D\nabla_{\Gamma_h} u_h \cdot \nabla_{\Gamma_h} b_j \,\mathrm{d}\mathcal{H}^{n-1}$$

Then notice:

$$\begin{aligned}
(w_h - v_h)\cdot\nabla b_i &= (w_h \cdot \nabla b_i - (v_h \cdot \nabla_{\Gamma_h} b_i + \underbrace{v_h \cdot (\nabla b_i \cdot \nu)\nu}_{= v_\nu \cdot (\nabla b_i \cdot \nu)\nu})) \\
&= w_h \cdot \nabla_{\Gamma_h} b_i + \underbrace{w_h \cdot (\nabla b_i \cdot \nu)\nu}_{= v_\nu \cdot (\nabla b_i \cdot \nu)\nu} - (v_h \cdot \nabla_{\Gamma_h} b_i + v_\nu \cdot (\nabla b_i \cdot \nu)\nu) \\
&= (w_h - v_h) \cdot \nabla_{\Gamma_h} b_i
\end{aligned}$$

Definition 4.4.2. For mesh points $\{x_i(t)\}_{i\in\mathcal{I}}$ on $\Gamma_h(t)$, define the matrix $\{T_{ij}\}_{i,j\in\mathcal{I}}$:

$$T_{ij}(t) \coloneqq \int_{\Gamma_h} b_i (w_h - v_h)\cdot\nabla_{\Gamma_h} b_j(x,t) \,\mathrm{d}\mathcal{H}^{n-1} \left(= \sum_{k\in\mathcal{I}} \int_{\Gamma_h} b_i (\partial_t x_k b_k - v(x_k) b_k) \cdot \nabla_{\Gamma_h} b_j \,\mathrm{d}\mathcal{H}^{n-1} \right)$$

Using the Galerkin approximation for u, with the mass and stiffness matrices M and S we obtain the matrix equation

$$M(t) f(t) = \frac{\mathrm{d}}{\mathrm{d}t} \Big(M(\cdot) u(\cdot) \Big)\Big|_t + DS(t)u(t) + T(t)u(t)$$

With a backwards Euler scheme the fully discrete problem is as follows.

Problem 4.4.1. *Given initial data u^0, timestep τ, solve for $n = 0, 1, 2, 3, ...$*

$$\begin{aligned}
&\frac{M^{n+1}u^{n+1} - M^n u^n}{\tau} + S^{n+1}u^{n+1} + T^{n+1}u^{n+1} = M^{n+1} f^{m+1} \\
&\implies \Big(\frac{1}{\tau} M^{n+1} + S^{n+1} + T^{n+1}\Big) u^{n+1} = \frac{1}{\tau} M^n u^n + M^{n+1} f^{n+1}
\end{aligned} \tag{4.6}$$

Chapter 5

Evolution laws for the membrane

We model the membrane of the cell by a moving embedded curve $\subset \mathbb{R}^2$. The movement itself is completely controlled by the imbalances between forces on the surface. We include the force given by the *surface tension* of the membrane, this would resist any stretching force of the boundary. It turns out this force, is described by the curvature of the membrane. We also couple this model to the chemical concentration model described in Chapter 4, by including a protrusive force acting normal to the membrane, (for example - if the concentration corresponded to deposits of Actin on a cell's membrane it would have this effect).

5.1 Dziuk method

This method (found in [4], and further analysis in[5]) describes the evolution of the curve by noticing that by definition of curvature (which we denote κ) we have the identity $\kappa\nu = \Delta_\Gamma x$. We also assume any kinetic constants to be unit for simplicity, we also assume we know the concentration on our surface (for all times $c : [0,T] \to \mathbb{R}$). The force balance can then be represented by the evolution law:

Problem 5.1.1. *For $T > 0$, $f : \mathbb{R} \to \mathbb{R}$ given, find $x : \mathbb{R}^2 \times [0,T] \to \mathbb{R}^2$ such that* $\forall\, t \in [0,T]$

$$\partial_t x = \Delta_\Gamma x + f(c)\nu \tag{5.1}$$

with initial data $x(\cdot,0) = x_0(\cdot)$

We may now formulate a weak formulation of our problem on Γ, for all test

functions ψ,

$$\int_\Gamma \partial_t x \cdot \psi - \Delta_\Gamma x \cdot \psi - f(c)\nu \cdot \psi \, \mathrm{d}x = 0$$

Notice the above the map x, denotes the identity mapping on the curve Γ. We now parametrise the curve with respect to a variable $\theta \in [0,1]$ and reuse x as the parametrisation mapping $x : [0,1] \times [0,T] \to \mathcal{G}$, a subtle difference. For arc length parameter s, and substituting $\Delta_\Gamma x = \partial_{ss} x$, in (5.1), our problem becomes

Problem 5.1.2. *For $T > 0$, $f : \mathbb{R} \to \mathbb{R}$ given, find $x : [0,1] \times [0,T] \to \mathbb{R}^2$ such that $\forall\, \theta \in [0,1]$, $t \in [0,T]$*

$$\partial_t x = \frac{1}{|x_\theta|} \left(\frac{x_\theta}{|x_\theta|} \right)_\theta + f(c) \left(\frac{x_\theta^\perp}{|x_\theta|} \right)$$

with initial data $x(\theta, 0) = x_0(\theta)$ and periodic boundary conditions $x(0,t) = x(1,t)$.

We choose a periodic boundary because we are considering a closed curve. We now write these equations in variational form. Let $\theta \in [0,1] = I$, for all ψ test functions

$$\int_I \partial_t x \cdot \psi |x_\theta| \, \mathrm{d}\theta = \int_I \left(\frac{1}{|x_\theta|} \left(\frac{x_\theta}{|x_\theta|} \right)_\theta \cdot \psi + f(c) \left(\frac{x_\theta^\perp}{|x_\theta|} \right) \cdot \psi) \right) |x_\theta| \, \mathrm{d}\theta$$

$$\text{integrate by parts} \implies 0 = \int_I \partial_t x \cdot \psi |x_\theta| + \frac{x_\theta \cdot \psi_\theta}{|x_\theta|} - f(c) x_\theta^\perp \cdot \psi \, \mathrm{d}\theta$$

So we have the variational formulation:

$$\int_I \partial_t x \cdot \psi |x_\theta| + \frac{x_\theta \cdot \psi_\theta}{|x_\theta|} \, \mathrm{d}\theta = \int_I f(c) x_\theta^\perp \cdot \psi \, \mathrm{d}\theta$$

5.1.1 Discretise in space and mass lumping

We now discretise in space, meshsize $h = \frac{1}{N}$ by taking nodes $\theta_k, k = 1, \ldots, N$ in $[0,1]$ and choose a surface finite element space with respect to the triangulation $\mathcal{T}_h$ on $\{\theta_k\}_k$ of our surface, $V_h = \{v \in C^0(\Gamma_h) \big| \, v|_T \text{ is an affine function } \forall\, T \in \mathcal{T}_h\} \subset H^1(\Gamma_h)$. Let $\psi_h = b_i \ \forall i = 1, 2, \ldots N$ be the finite element basis elements of the space V_h (the finite element space is assumed independent of time unless one were doing mesh adaption techniques). The discrete space problem reads:

Problem 5.1.3. *For $T > 0$, $f : \mathbb{R} \to \mathbb{R}$ given, find $x_h \in V_h \, \forall t \in [0,T]$, such that $\forall\, \psi_h \in V_h$ and $\forall\, \theta \in I$, $t \in [0,T]$*

$$\int_I \partial_t x_h \cdot \psi_h |x_{h\theta}| + \frac{x_{h\theta} \cdot \psi_{h\theta}}{|x_{h\theta}|} \, d\theta = \int_I f(c_h) x_{h\theta}^\perp \cdot \psi_h \, d\theta$$

with initial data $x_h(\theta,0) = x_{0h}(\theta)$ *and periodic boundary conditions* $x_h(0,t) = x_h(1,t)$.

In practise however we use the technique known as 'mass lumping' which proceeds to use in place of the standard finite element interpolation function which we denoted $J_h(x) \coloneqq x_h$ above, but we use a further interpolation function $I_h : C^0 \to V_h$ defined by $I_h(x)(\theta_i) \coloneqq x(\theta_i)$. Without mass lumping we obtain, for some arbitrary function $u_h \in V_h$ with the ansatz $u_h = \sum_j u_j(t)b_j(\theta)$ that, $\forall i = 1, \dots, N$

$$\int_0^1 u_h b_i |x_{h\theta}| \,\mathrm{d}\theta = \sum_j u_j(t) \int_0^1 b_j(\theta) b_i(\theta) |x_{h\theta}| \,\mathrm{d}\theta = \sum_j M_{ij} u_j(t)$$

Where M_{ij} is a standard weighted mass matrix by $|x_{h\theta}|$.

With the mass lumping however we would be considering this problem:

$$\begin{aligned}
\int_0^1 I_h(u_h b_i)|x_{h\theta}| \,\mathrm{d}\theta &= \int_0^1 \sum_j u_j(t) I_h(b_j b_i)|x_{h\theta}| \,\mathrm{d}\theta \\
&= \sum_k \sum_j u_j(t) I_h(b_i b_k)(\theta_k)|x_{h\theta}| \\
&= \sum_k \sum_j u_j(t) \underbrace{b_j(\theta_k) b_i(\theta_k)}_{\delta_{ij}} |x_{h\theta}| \\
&= \sum_k u_i(t) b_i(\theta_k)|x_{h\theta}| \\
&= \int_0^1 u_i(t) b_i(\theta)|x_{h\theta}| \,\mathrm{d}\theta
\end{aligned}$$

Notice how this will produce a mass matrix $\overline{M}$ which is weighted by $|x_{h\theta}|$, but most importantly it will be a diagonal matrix - making operations even more efficient.

We may calculate the integral given from the mass lumping explicitly, as we have a linear interpolated SFEM - and this can be seen in the appendix.

5.1.2 Discretise in time

Then discretise in time with timestep τ, to obtain a fully discrete scheme:

Problem 5.1.4. *Solving for* $n = 1, 2, 3, \dots$
for $f : \mathbb{R} \to \mathbb{R}$, $\tau > 0$ *small and* x_h^{n-1} *given, find* $x_h^n \coloneqq x_h(t_n) \in V_h$, $(t_n = n\tau)$ *such*

that $\forall\, \psi_h \in V_h$ *and* $\forall\, \theta \in I$

$$\int_I \frac{x_h^n - x_h^{n-1}}{\tau} \cdot \psi_h |x_\theta^{n-1}| + \frac{x_{h\theta}^n \cdot \psi_{h\theta}}{|x_{h\theta}^{n-1}|}\, d\theta = \int_I f(c_h^{n-1}) x_{h\theta}^{\perp n-1} \cdot \psi_h \, d\theta$$

with initial data $x_h(\theta, 0) = x_h^0(\theta)$ *and periodic boundary conditions* $x_h^n(0, t_n) = x_h^n(1, t_n)$.

Denoting $x_h = \begin{pmatrix} y_h \\ z_h \end{pmatrix}$ (coefficients with respect to the finite element basis $(b_i)_i$). We call $|x_{h\theta}^{n-1}| = g_h^{n-1}$ we may construct:

$$\left(M_{g_h}^{n-1}\right)_{i,j} = \int_I b_i^{n-1} b_j^{n-1} g_h^{n-1} d\theta \quad \text{and} \quad \left(S_{g_h}^{n-1}\right)_{i,j} = \int_I \frac{\nabla b_i^{n-1} \cdot \nabla b_j^{n-1}}{g_h^{n-1}} d\theta$$

the weighted mass and weighted stiffness matrices, similarly we may construct the diagonalised 'mass lumping' versions. Then we represent our equation in matrix form:

$$\begin{pmatrix} \frac{1}{\tau} M_{g_h}^{n-1} & 0 \\ 0 & \frac{1}{\tau} M_{g_h}^{n-1} \end{pmatrix} \begin{pmatrix} y_h^n \\ z_h^n \end{pmatrix} + \begin{pmatrix} S_{g_h}^{n-1} & 0 \\ 0 & S_{g_h}^{n-1} \end{pmatrix} \begin{pmatrix} y_h^n \\ z_h^n \end{pmatrix} = \begin{pmatrix} \frac{1}{\tau} M_{g_h}^{n-1} & 0 \\ 0 & \frac{1}{\tau} M_{g_h}^{n-1} \end{pmatrix} \begin{pmatrix} y_h^{n-1} \\ z_h^{n-1} \end{pmatrix} + \begin{pmatrix} f(y^{n-1}) \\ f(z^{n-1}) \end{pmatrix} \tag{5.2}$$

5.2 Barrett Garcke Nürnberg method

We now consider the defining equation for the curvature as a coupled system which separates out the motion in the normal and the tangential direction. Rather than restricting the motion to be entirely in the normal direction (as with Dziuk), the equation will now admit solutions that may also have a tangential component of the velocity governed by the curvature (surface tension) flow, as seen given in the second equation. We consider the following problem:

Problem 5.2.1. *For* $T > 0$, $f : \mathbb{R} \to \mathbb{R}$ *given, find* $x : \mathbb{R}^2 \times [0, T] \to \mathbb{R}^2$ *such that* $\forall\, t \in [0, T]$

$$\begin{cases} \partial_t x &= \kappa\nu + f(c)\nu \\ \kappa\nu &= \Delta_\Gamma x \end{cases} \quad \textit{which becomes} \quad \begin{cases} \partial_t x \cdot \nu &= \kappa + f(c) \\ \kappa\nu &= \Delta_\Gamma x \end{cases}$$

with initial data $x(\cdot, 0) = x_0(\cdot)$

as in the Dziuk scheme above we write our equations in variational form, for all ψ test fucntions.

$$\begin{cases} \displaystyle\int_\Gamma \partial_t x \cdot \nu\psi - \kappa\psi \,\mathrm{d}x &= \displaystyle\int_\Gamma f(c)\psi \,\mathrm{d}x \\ \displaystyle\int_\Gamma \kappa\phi \cdot \nu + \Delta_\Gamma x \cdot \phi \,\mathrm{d}x &= 0 \end{cases}$$

As before we can parametrise our equations to obtain the parametrised formulation with respect to $\theta \in [0,1]$ and recall the notation for the parametrisation mapping is given by $x : [0,1] \times [0,T] \to \mathbb{R}^2$.

$$\begin{cases} \partial_t x \cdot \dfrac{x_\theta^\perp}{|x_\theta|} &= \kappa + f(c) \\ \kappa \dfrac{x_\theta^\perp}{|x_\theta|} &= \dfrac{1}{|x_\theta|}\left(\dfrac{x_\theta}{|x_\theta|}\right)_\theta \end{cases}$$

Integration by parts yields the parametrised version of the weak form:

$$\begin{cases} \displaystyle\int_I \left(\partial_t x \cdot \frac{x_\theta^\perp}{|x_\theta|}\psi - \kappa\psi\right)|x_\theta| \,\mathrm{d}\theta &= \displaystyle\int_I f(c)\psi|x_\theta| \,\mathrm{d}\theta \\ \displaystyle\int_I \left(\kappa\phi \cdot \frac{x_\theta^\perp}{|x_\theta|} + \frac{x_\theta \cdot \phi_\theta}{|x_\theta|^2}\right)|x_\theta| \,\mathrm{d}\theta &= 0 \end{cases}$$

5.2.1 Discretise in space

Then we discretise in space. We use the same space $V_h = \{v \in C^0(\Gamma_h) \big| \, v|_T \text{ affine } \forall\, T \in \mathcal{T}_h\} \subset H^1(\Gamma_h)$, as in the Dziuk method. We obtain,

Problem 5.2.2. *For $T > 0$, $f : \mathbb{R} \to \mathbb{R}$ given, find $x_h \in V_h \,\forall t \in [0,T]$, such that $\forall\, \psi_h, \phi_h \in V_h$ and $\forall\, \theta \in I$, $t \in [0,T]$*

$$\begin{cases} \displaystyle\int_I \partial_t x_h \cdot x_{h\theta}^\perp \psi_h - \kappa_h \psi_h |x_{h\theta}| \, d\theta &= \displaystyle\int_I f(c)_h \psi_h |x_{h\theta}| \, d\theta \\ \displaystyle\int_I \kappa_h \phi_h \cdot x_{h\theta}^\perp + \frac{x_{h\theta} \cdot \phi_{h\theta}}{|x_{h\theta}|} \, d\theta &= 0 \end{cases}$$

with initial data $x_h(\theta,0) = x_{0h}(\theta)$ and periodic boundary conditions $x_h(0,t) = x_h(1,t)$.

With regards to mass lumping an identical procedure has been applied to the mass and stiffness matrices as in subsection §5.1.1. So our problem may be formulated with respect to further discretisation function $I_h : C^0 \to V_h$ such that $I_h(x)(\theta_i) = x(\theta_i)$.

$$\begin{cases} \displaystyle\int_I I_h(\partial_t x_h \cdot \psi_h) x_{h\theta}^{\perp} - \kappa_h \psi_h |x_{h\theta}| \,\mathrm{d}\theta & = \displaystyle\int_I I_h(f(c)_h \psi_h)|x_{h\theta}| \,\mathrm{d}\theta \\ \displaystyle\int_I \kappa_h \phi_h \cdot x_{h\theta}^{\perp} + \frac{I_h(x_{h\theta} \cdot \phi_{h\theta})}{|x_{h\theta}|} \,\mathrm{d}\theta & = 0 \end{cases}$$

This can be incorporated into the formulation, and should be taken into account as a further approximation step in the method.

5.2.2 Discretise in time and the scheme

Finally discretise in time to give the scheme, We use an iterative update method, thus solve for $(x_h^n - x_h^{n-1})$, as the updating variable:

Problem 5.2.3. *Solving for $n = 1, 2, 3, \ldots$*
for $f : \mathbb{R} \to \mathbb{R}$, $\tau > 0$ small and x_h^{n-1} given, find $x_h^n \coloneqq x_h(t_n) \in V_h$, $(t_n = n\tau)$ such that $\forall\, \psi_h, \phi_h \in V_h$ and $\forall\, \theta \in I$

$$\begin{cases} \displaystyle\int_I \frac{x_h^n - x_h^{n-1}}{\tau} \cdot x_{h\theta}^{\perp\, n-1} \psi_h - \kappa_h^n \psi_h |x_{h\theta}^{n-1}| \, d\theta & = \displaystyle\int_I f(c_h^{n-1}) \psi_h |x_{h\theta}^{n-1}| \, d\theta \\ \displaystyle\int_I \kappa_h^n \phi_h \cdot x_{h\theta}^{\perp\, n-1} + \frac{(x_{h\theta}^n - x_{h\theta}^{n-1}) \cdot \phi_{h\theta}}{|x_{h\theta}^{n-1}|} \, d\theta & = -\displaystyle\int_I \frac{x_{h\theta}^{n-1} \cdot \phi_{h\theta}}{|x_{h\theta}^{n-1}|} \, d\theta \end{cases}$$

with initial data $x_h(\theta, 0) = x_h^0(\theta)$ and periodic boundary conditions $x_h^n(0, t_n) = x_h^n(1, t_n)$.

Taking $\psi_h, \phi_h = b_i \; \forall i = 1, 2, \ldots N$ as the finite element basis elements of the space V_h and denoting $x_h = \begin{pmatrix} y_h \\ z_h \end{pmatrix}$ (coefficients with respect to this basis). We call $|x_{h\theta}^{n-1}| = g_h^{n-1}$ and create:

$$\left(N_{x_h}^{n-1}\right)_{i,j} = \int_I b_i \cdot b_j \, x_{h\theta,j}^{\perp\, n-1} |x_{h\theta}^{n-1}| d\theta$$

The system may then be represented in matrix form (F_h is the matrix that represents the right hand side forcing on κ).

$$\begin{pmatrix} -\tau M_{g_h}^{n-1} & N_{y_h}^{n-1} & N_{z_h}^{n-1} \\ N_{y_h}^{\perp\, n-1} & S_{g_h}^{n-1} & 0 \\ N_{z_h}^{\perp\, n-1} & 0 & S_{g_h}^{n-1} \end{pmatrix} \begin{pmatrix} \kappa_h^n \\ y_h^n - y_h^{n-1} \\ z_h^n - z_h^{n-1} \end{pmatrix} = \begin{pmatrix} \tau F_h & N_{y_h}^{n-1} & N_{z_h}^{n-1} \\ 0 & -S_{g_h}^{n-1} & 0 \\ 0 & 0 & -S_{g_h}^{n-1} \end{pmatrix} \begin{pmatrix} \kappa_h^{n-1} \\ y_h^{n-1} \\ z_h^{n-1} \end{pmatrix} \tag{5.3}$$

5.2.3 Consequence of tangential motion

Remark. Now we have seen the introduction of a tangential component into the evolution we can see it is required that one uses an alternative discretisation to the ESFEM presented in Section 4.3. This alternative must take into account the added motion across the surface that is not governed by just the surface PDE, and consequentially 4.4 is used in the coupling implementation.

Remark. Section 3.3 presented a method of caluclation of the knot energy using a proportional technique. As the BGN-ALE scheme we propose has a structure that has contains a tangential flow, and moreover this flow equidistributes points around the surface, it is an ideal candidate for this proposed method.

Chapter 6

Implementation and Numerics of moving curves

The numerical simulations were performed on `MATLAB v2013b`

6.1 Implementational structure

The overall algorithm that we wish to implement is the following:

Inputs

- Initial shape of body (corresponding to x_h^0 in Chapter 5.1.2).
- Initial concentrations of quantity u (corresponding to u^0 in Chapter 4.3).
- Number of segments of curve $N(=\frac{1}{h})$.
- Timestep τ, for stability we will assume in the numerics later that this is $\mathcal{O}(h^2)$.
- Initial forcing coefficient f for the surface evolution scheme (again see 5.1.2).

Main steps

- Perform one timestep of the surface evolution scheme (either Dziuk (5.2) or Barrett Garcke Nürnberg (5.3)) using the forcing quantity given initially or constructed from the concentration of the conserved surface quantity u (from previous timestep).
- Calculate the discrete Möbius energy of this evolved surface using (2.5).

- Calculate the new concentration of quantity u on the new surface using derived matrix equation (4.4) (or if using BGN - the equation (4.6)).

Outputs at step n

- The position of the curve at time $n\tau$ - i.e x_h^n .
- The concentration of our quantity on the curve - u^n .
- The (discrete) Möbius energy of the curve at time $n\tau$.

6.2 Detection

Finally we must state how we going to indicate the detection of an intersection itself. We use a two step process, an *activation* of the sensor and then - once activated, we use a *detector* to decider whether a self intersection has occured.

In the continuum model we get an explosion of the energy, and thus we would seek out a significant energy spike in our discrete model. The size of this peak will become more pronounced with increased timesteps and meshsize, due to the increased accuracy of the model and so we would allow our model to 'assume' that a smooth steep rise in energy would correspond to an approach to self-intersection, then a peak at the point of self intersection.

To this end, we could implement something as follows: we record a running mean or baseline, and the standard deviation of the energy. At timestep n we have

$$M(n) = \frac{1}{n}\sum_{i=1}^{n} E(p_N(t_i)), \quad \text{and} \quad S(n) = \sqrt{\sum_{i=1}^{n}(E(p_N(t_i)) - M(n))^2}$$

This is what we measure our significance of peak with, using a threshold α so that if $E(p_N(t_n)) \geq M(n) + \alpha S(n)$, we may switch on the sensor to detect a peak in our energy (for example let $\alpha = 3$). We do this numerically, and simply require if $E(p_N(t_n)) - E(p_N(t_{n-1})) < 0$, then we have obtained a peak. The motivation of this is that we wait for a "statistically significant" value of the energy given the behaviour of it previously.

This will be effective as once the energy starts to spike, it becomes a strictly increasing function (as it approximates a sharp interface) until it has acheived intersection.

6.3 Setup and framework

For the testing we use a couple of different initial configurations. We approximate three different shapes, firstly the unit radius circle, and secondly, an ellipse with diameter ratio of $1 : 2.5$ and thirdly what we shall call the "C-shape" with outer radius a and radius of the width of the cell is r, and angle of rotation θ (the parametrisation of these shapes can be found in the appendix).

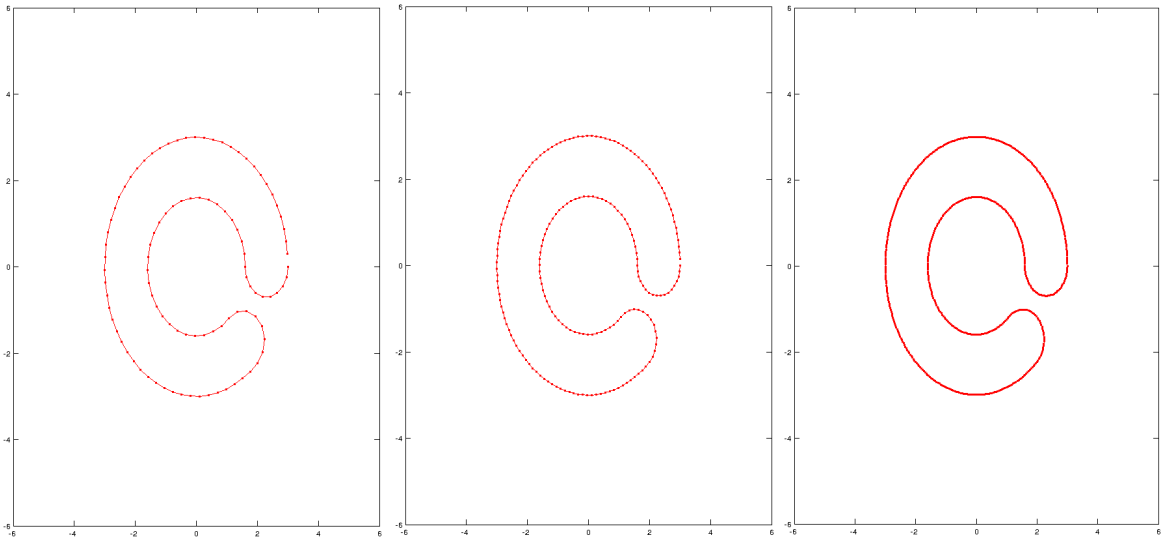

Figure 6.1: *C-shaped membrane approximation with N=100, 200 and 600 points,*$a = 3$, $r = 0.7, \theta = \pi + 2.3$

The initial force that we apply for the purpose of the force term in the surface PDE is initially given as $2+2cos(\pi t)$ i.e at timestep $n = 0$ has value 4 at the beginning and end of the parametrisation interval and 0 in the middle. For example on the C shape curve in Figure 6.1 this corresponds to the highest force value being the arm centered about the points $(a - r, 0)$.

6.3.1 Dziuk scheme

We present two tests to demonstrate the Dziuk scheme, first with an equidistributed initial distribution and secondly with an initial distribution designed to show possible flaws between the evolution and the Möbius energy's ability to detect a self-intersection.

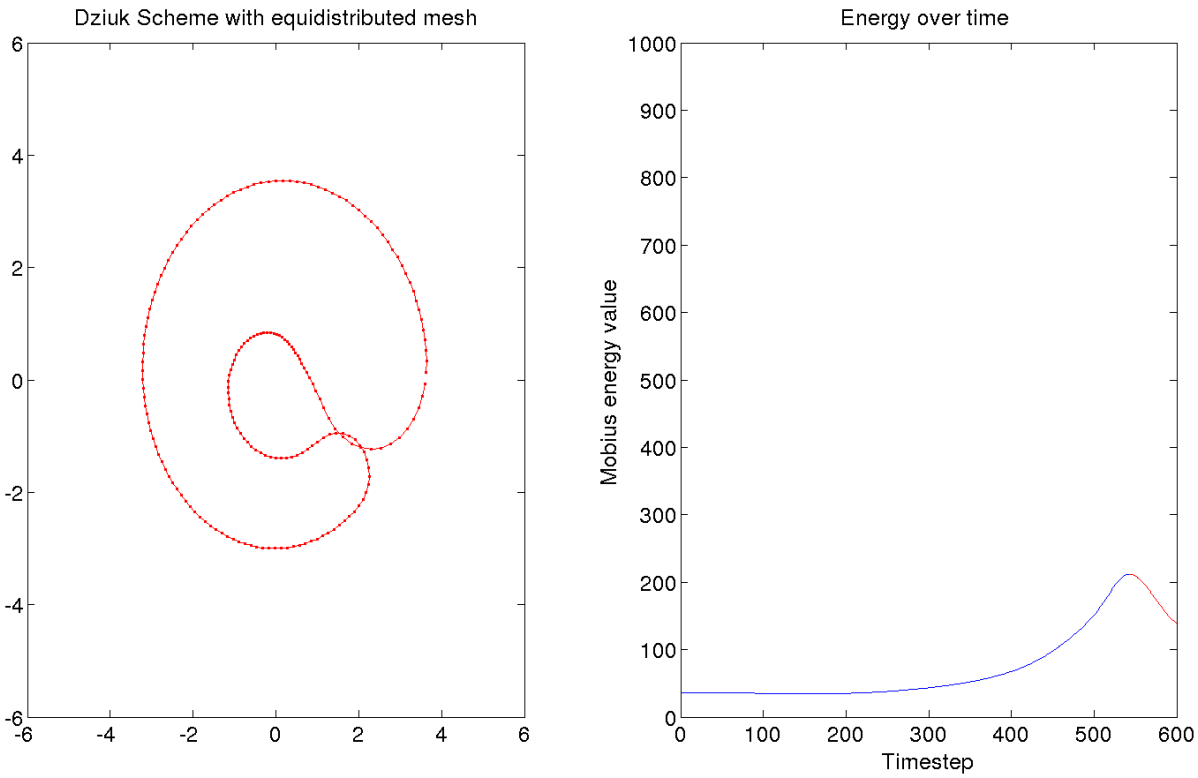

Figure 6.2: *the left shows the final mesh distribution after 600 timesteps. On the right we see the graph of the energy peak at a detected intersection.* $N = 200$, $a = 3$, $r = 0.7$, $\theta = \pi + 2.3$

Now we us another distributed C-shape to demonstrate a difficult scenario for the Dziuk scheme. That is, one where there is a larger concentration away from the areas of self intersections. The initial distribution is given on the next page:

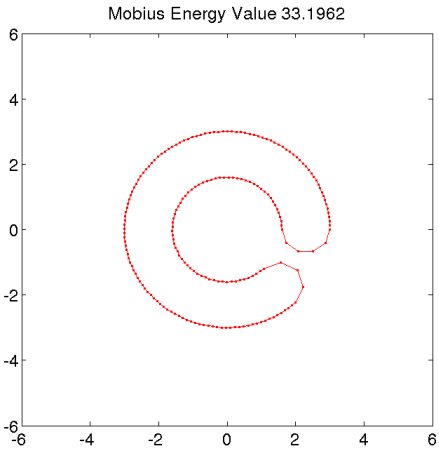

With this initial start mesh distribution we see a significant change in the effectiveness of the scheme. As the scheme is unable to equidistribute points effectively (motion in the normal direction of the surface only) we see a lack of resolution below and an intersection is unable to be detected (the peak is not sharp enough to breach the green horizontal threshold).

Figure 6.3: $N = 200$, $a = 3$, $r = 0.7$, $\theta = \pi + 2.3$

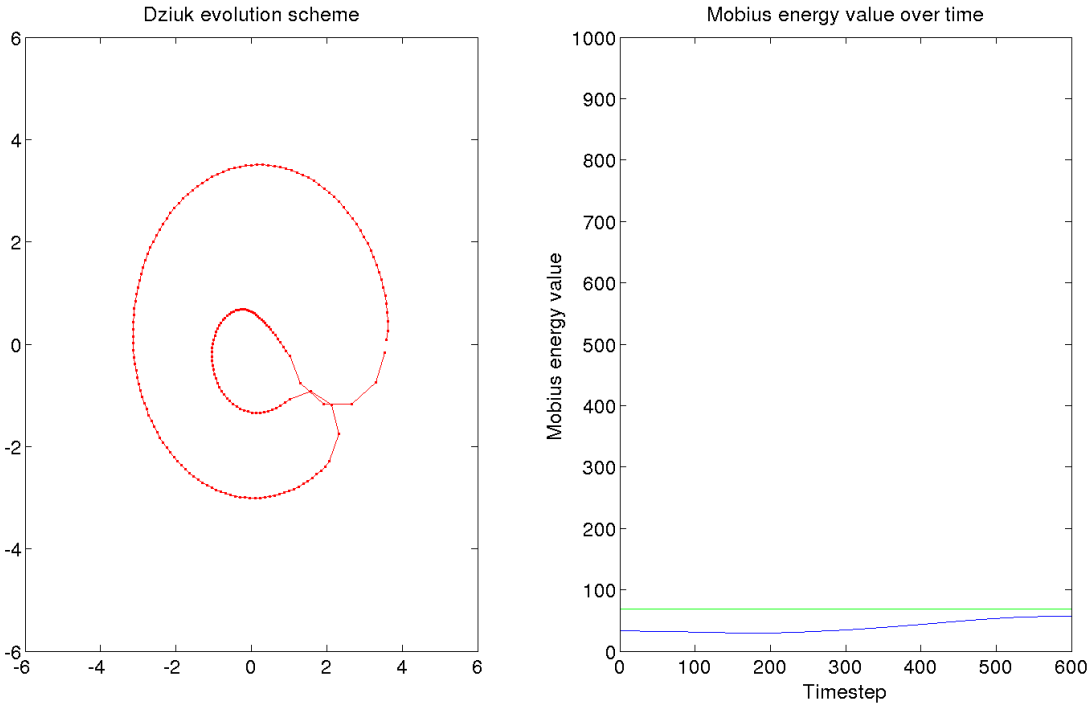

Figure 6.4: *the left shows the final mesh distribution after 600 timesteps - and visually showing an intersection. On the right we see the graph of the energy that has not detected a peak. (The green bar represents the threshold for detection)*$N = 200$, $a = 3$, $r = 0.7$, $\theta = \pi + 2.3$

6.3.2 BGN scheme

We demonstrate the benefit of equidistribution property of the BGN-ALE ESFEM scheme over that of Dziuk with the following evolution of the C-shape with initial distribution given by (6.3).

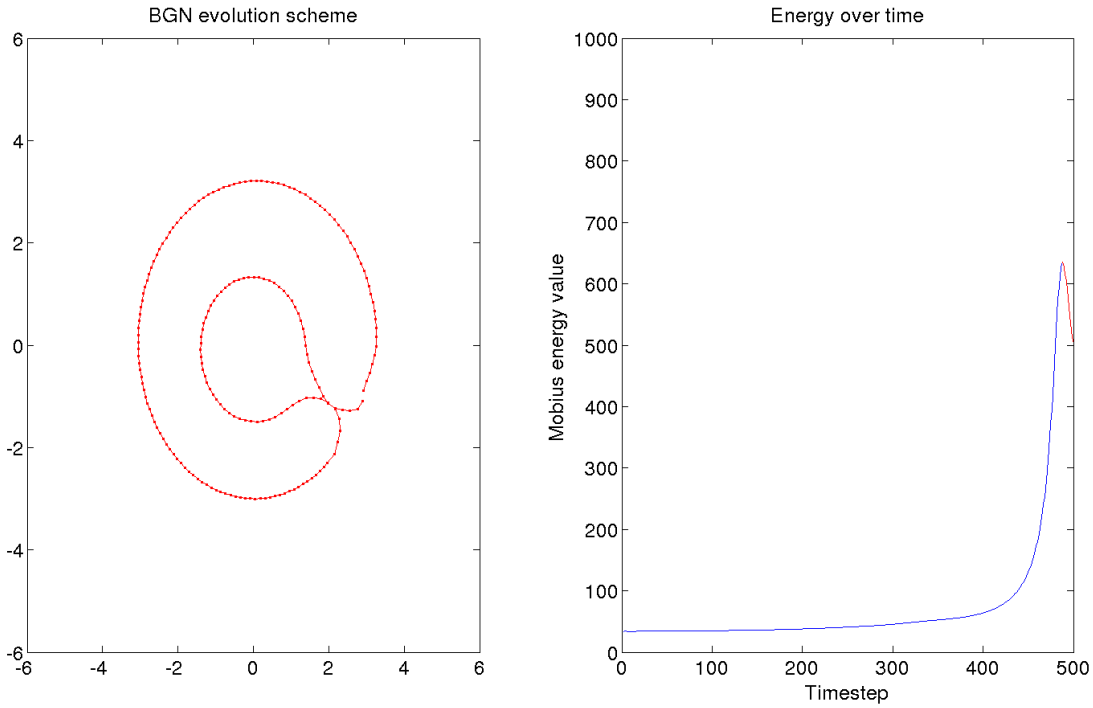

Figure 6.5: *the left shows the final mesh distribution after 500 timesteps. On the right we see the graph of the energy peak at a detected intersection.* $N = 200$, $a = 3$, $r = 0.7$, $\theta = \pi + 2.3$

Note that there is a well pronounced peak and the distribution is near equilibrium already. Also notice that this does alter the appearence and evolution direction of the curve. Also I have not included the BGN evolution from the initially equidistributed mesh points because the behaviour is quite stable under this initial condition, and thus the motion is similar.

6.3.3 Proportional geodesic distance calculation

One other idea that was mentioned with regards to the BGN scheme and efficiently calculating the Möbius energy was the use of proportional summation of segments of the curve to calculate the geodesic distances between points (which consisted of

the bulk of the calculation time). This enforced a bound on the mesh size range for any given curve by a number $q = \frac{q_{\max}}{q_{\min}}$, then these bounds may be used to calculate a bound of the energy from above or below.

A difficulty presented itself with this method was how to determine a ratio q that was small enough to have enough information to determine an energy spike, and large enough to still remain efficient. Three different effects are observed regarding this balance of efficiency and accuracy. As previously all simulations have been conducted with $N = 200$, $a = 3$, $r = 0.7$, $\theta = \pi + 2.3$.

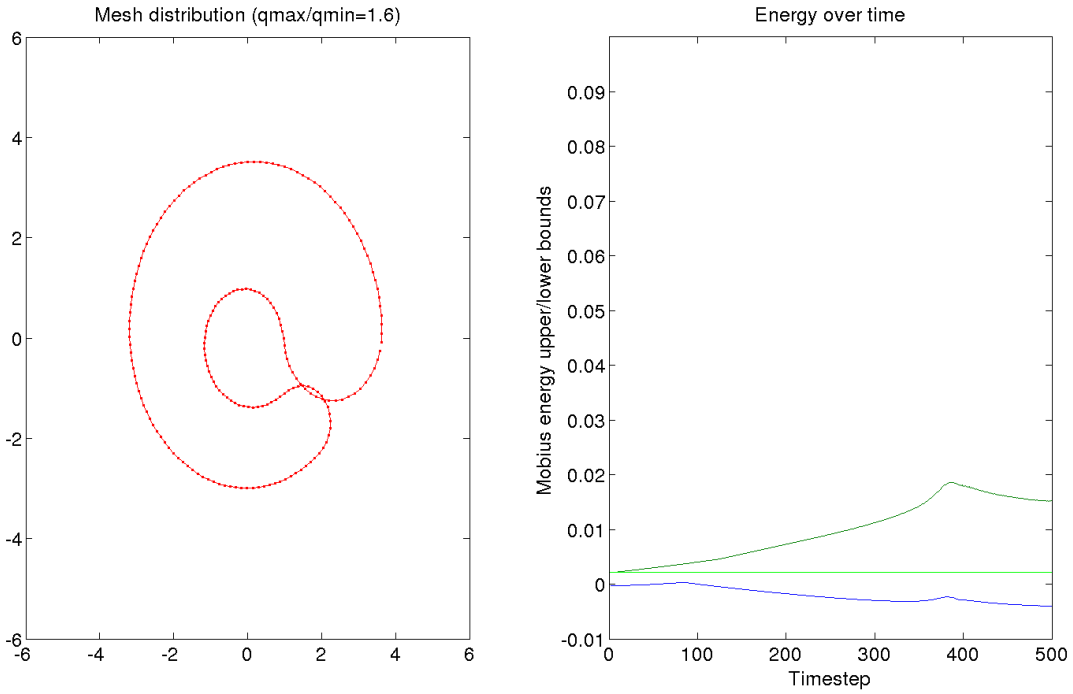

Figure 6.6: *($q = 1.6$) On the right we see no intersection has been detected - the horizontal green bar shows the threshhold for detection*

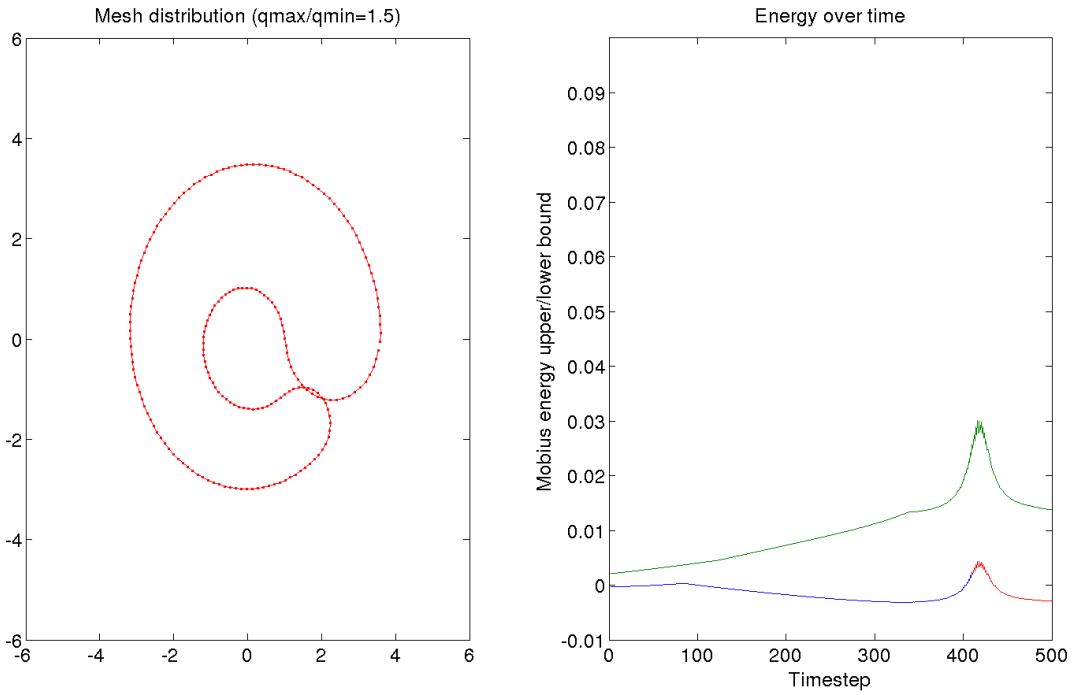

Figure 6.7: *($q = 1.5$) An intersection has been detected but with wide energy bound*

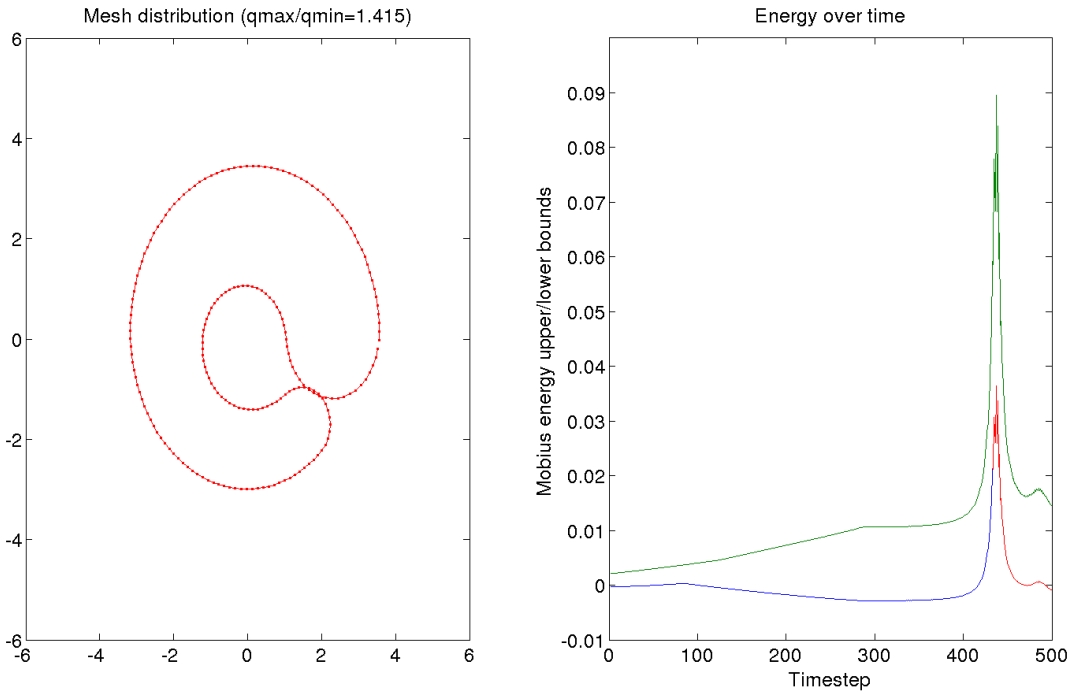

Figure 6.8: *($q = 1.415$) A detected intersection with narrow energy bounds*

The first figure 6.6 has wide bounds on the energy and it is too inaccurate to even determine whether an intersection has taken place, in this scenario the energy has not yet required remeshing and the calculation is very quick.

The next scenario, figure 6.7,undergoes some remeshing steps that make the energy bounds slightly tighter but takes more time, and there is enough of a peak at timestep 440 for the model to determine an intersection. However the bounds are still too wide, and the energy in between these bounds could have not suffered any perturbation and so from the graph there is not enough information given to determine whether we have really witnessed a self-intersection.

The final graph 6.8 does have a sharp peak and this is sharp enough for there to be no question as to whether an energy bounded in between the curve plotted had indeed spiked. This therefore is the optimal scenario, however if we used $q \leq 1.415$ as a tolerance for the BGN-ALE method, for every timestep we had to perform hundreds or more remeshing steps to acheive this q. These remesh steps are costly when performed so many times and this evolution took even longer than the original evolution without.

If one could use another equidistribution method such as using a harmonic map calculation at every step (numerically solving a relatively uncomplicated PDE - whose solution provides a map that equidistributes mesh points), this method could be used very efficiently. An example of their use can be found in [13]. We merely propose this scheme in this project due to time constraints.

6.3.4 Linear cutoff and smoothing

We first demonstrate that we can use very small cutoff values of θ_1 and θ_2 without effecting an energy curve of a C-shape intersection. We use the values $N = 300$, $a = 3$, $r = 0.7$, $\theta = \pi + 2.3$ for the initial shape.

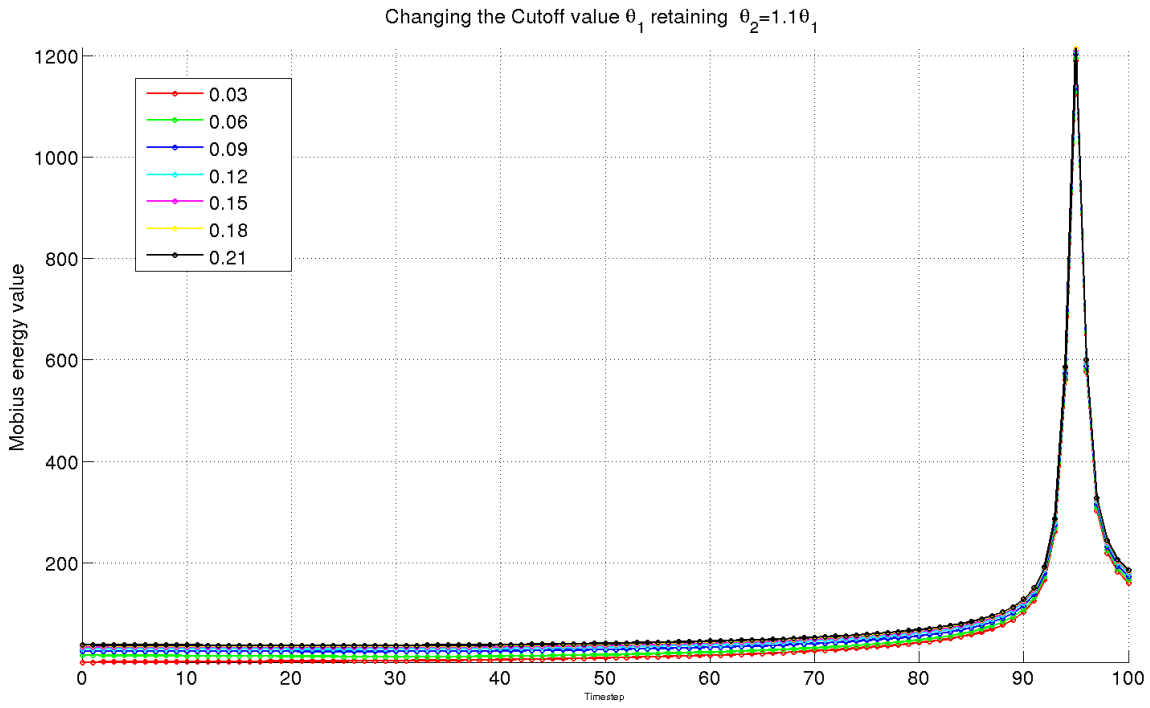

Figure 6.9: *we increase* $\theta_1 = 0.03, 0.06 \ldots, 0.21$ *keeping* $\theta_2 = 1.1\theta_1$

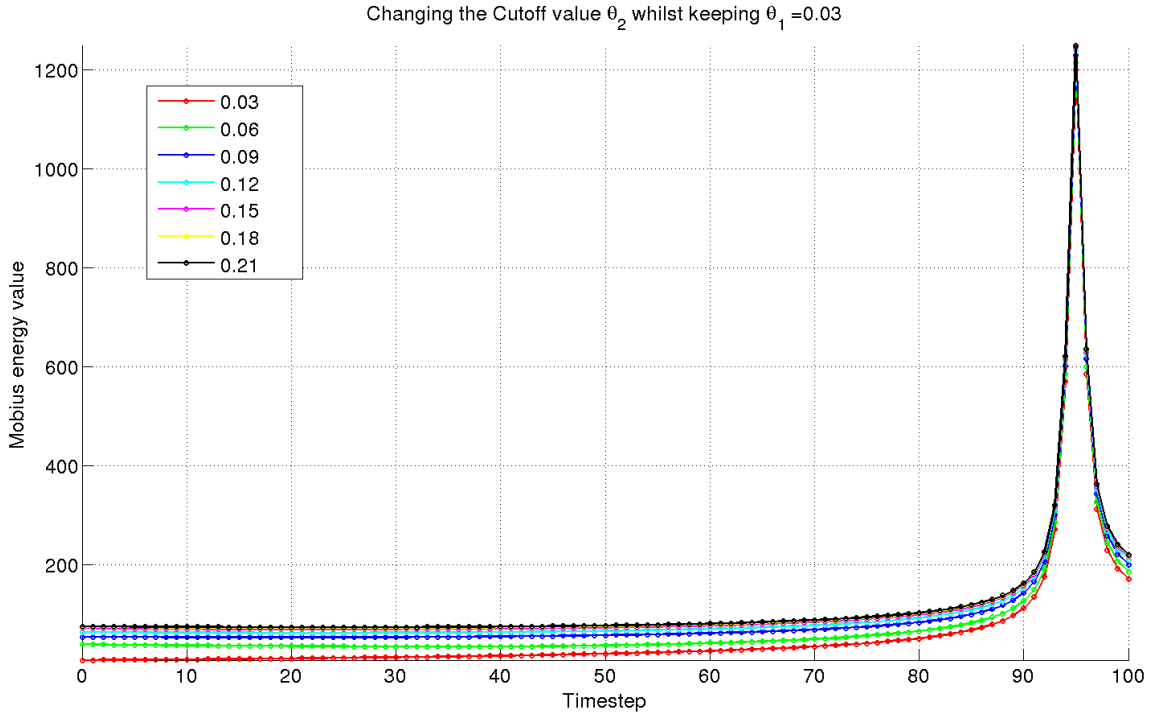

Figure 6.10: *we increase* $\theta_2 = 0.03, 0.06 \ldots, 0.21$ *keeping* $\theta_1 = 0.03$.

Although the energy is effected very little, having a large cutoff increases efficiency a vast amount as you can use (for large N) just a few points of interest close and the geodesic calculation as despite staying $\mathcal{O}(N^3)$, we reduce the bound constant significantly.

Finally, we plot an error graph of another intersecting scenario, but we now look at the difference between using a smoothed and unsmoothed energy. The intersection takes place at 880^{th} timestep.

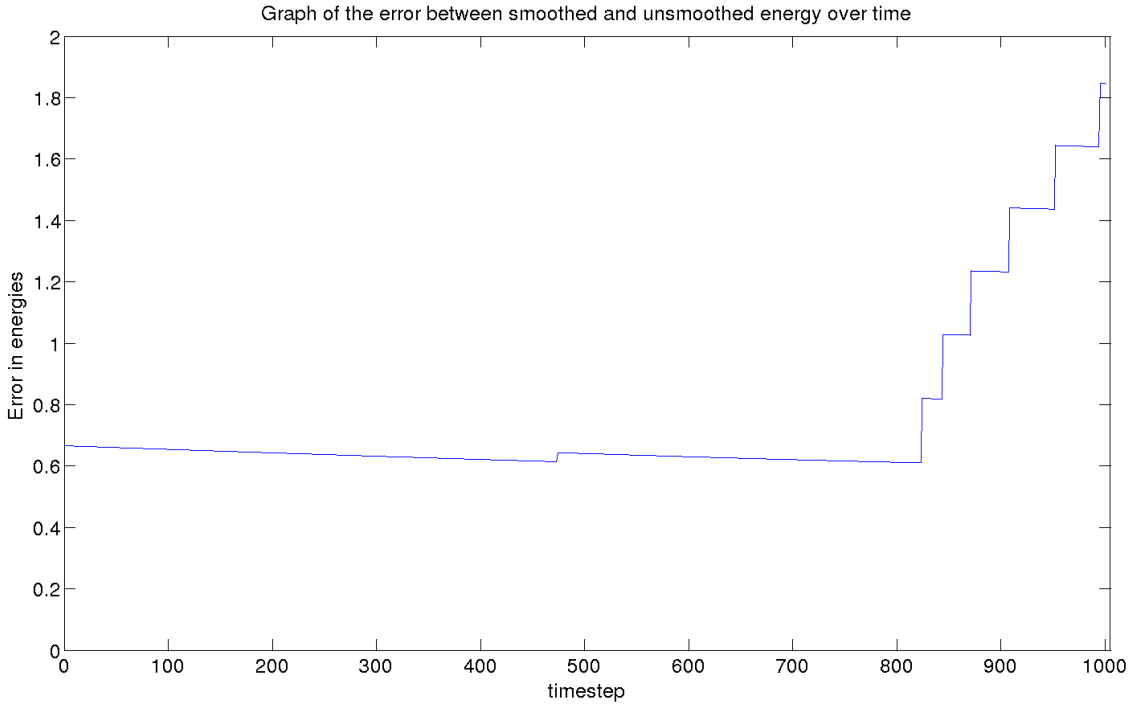

Figure 6.11: *Showing the difference between a smoothed and unsmoothed energy during a typical intersecting evolution. (intersection occurs at step 880). We have* $\theta_1 = 0.05$, $\theta_2 = 0.06$.

As anticipated, considering the values of the energy at the start is $E = 36.070$, and around the point of intersection we have $E = 1706.8898$. The difference of smoothing is negligible. The cutoff function also has little effect, so long as the smoothing radius is lower than the minimum cutoff. The step-like nature of the graph is due to the curvature and length of the curve to altering over time. This causes a jump in our smoothing function (involves a floor function) or the cutoff function to effect more or less points, giving a discrete step in the error.

Chapter 7

An extension: Prevention of self-intersections

7.1 The Energy variation

Recall our energy is given by the parametrisation of a membrane $\Gamma \subset \mathbb{R}^2$ by the function $\gamma : [0,1] \to \Gamma$. We denote the geodesic/arc distance between two points on the curve by $d_\gamma(x,y)$, then:

$$E(\gamma) \coloneqq \iint_{[0,1]^2} \left(\frac{1}{|\gamma(x) - \gamma(y)|^2} - \frac{1}{d_\gamma(x,y)^2} \right) |\gamma'(x)||\gamma'(y)| \,\mathrm{d}x \,\mathrm{d}y$$

We wish to consider the variation of this quantity denoted δE,with respect to the variation v

$$\langle \delta E(u), v \rangle = \int \frac{\delta E}{\delta u(r)} v(r) \,\mathrm{d}r = \lim_{\varepsilon \downarrow 0} \frac{E(u(r) + \varepsilon v(r)) - E(u(r))}{\varepsilon} = \frac{\mathrm{d}}{\mathrm{d}\varepsilon} E(u + \varepsilon v) \bigg|_{\varepsilon = 0}$$

Then the first variation of the energy functional is denoted (with $\delta u(r) = \varepsilon v(r)$, the variation of u):

$$\delta E(u) \coloneqq \int \frac{\delta E}{\delta u(r)} \delta u(r) \,\mathrm{d}r$$

Thus we split our energy into 3 parts:

$$\langle \delta E(\gamma), \varphi \rangle \coloneqq \iint_{[0,1]^2} \frac{\mathrm{d}}{\mathrm{d}\varepsilon} \Bigg[\Big(\overbrace{\frac{1}{|\gamma(x)-\gamma(y)+\varepsilon(\varphi(x)-\varphi(y))|^2}}^{\mathbb{A}} - \overbrace{\frac{1}{d_{\gamma+\varepsilon\varphi}(x,y)^2}}^{\mathbb{B}} \Big) \cdot \underbrace{|\gamma'(x)+\varepsilon\varphi'(x)||\gamma'(y)+\varepsilon\varphi'(y)|}_{\mathbb{C}} \Bigg] \mathrm{d}x\,\mathrm{d}y \Bigg|_{\varepsilon=0}$$

terms $\mathbb{C}$ and $\mathbb{A}$ can be dealt with relatively easily:

$$\mathbb{C}\colon \quad \frac{\mathrm{d}}{\mathrm{d}\varepsilon}\Big(|\gamma'(x)+\varepsilon\varphi'(x)||\gamma'(y)+\varepsilon\varphi'(y)|\Big)\Big|_{\varepsilon=0} = \frac{\langle \gamma'(x), \varphi'(x)\rangle}{|\gamma'(x)|}|\gamma'(y)| + \frac{\langle \gamma'(y), \varphi'(y)\rangle}{|\gamma'(y)|}|\gamma'(x)|$$

$$\mathbb{A}\colon \quad \frac{\mathrm{d}}{\mathrm{d}\varepsilon}\Big(\frac{1}{|\gamma(x)-\gamma(y)+\varepsilon(\varphi(x)-\varphi(y))|^2}\Big)\Big|_{\varepsilon=0} = -2\frac{\langle \gamma(x)-\gamma(y), \varphi(x)-\varphi(y)\rangle}{|\gamma(x)-\gamma(y)|^4}$$

For the final term, we write out in full:

$$d_{\gamma+\varepsilon\varphi}(x,y) = \min\Big\{ \underbrace{\int_x^y |\gamma'(s)+\varepsilon\varphi'(s)|\,\mathrm{d}s}_{\mathbb{B}_1(\varepsilon)} \ , \ \underbrace{\int_0^x |\gamma'(s)+\varepsilon\varphi(s)|\,\mathrm{d}s + \int_y^1 |\gamma'(s)+\varepsilon\varphi(s)|\,\mathrm{d}s}_{\mathbb{B}_2(\varepsilon)} \Big\}$$

Then, the derivatives of each quantity are, (in a similar way to $\mathbb{C}$)

$$\begin{aligned}
&\frac{\mathrm{d}}{\mathrm{d}\varepsilon}\min\{\mathbb{B}_1(\varepsilon), \mathbb{B}_2(\varepsilon)\} \\
&\quad = \begin{cases} \dfrac{\mathrm{d}}{\mathrm{d}\varepsilon}\mathbb{B}_1(\varepsilon) = \displaystyle\int_x^y \frac{\langle \gamma'(s), \varphi'(s)\rangle}{|\gamma'(s)+\varepsilon\varphi'(s)|}\,\mathrm{d}s & \text{if } \mathbb{B}_1(\varepsilon) < \mathbb{B}_2(\varepsilon) \\ \dfrac{\mathrm{d}}{\mathrm{d}\varepsilon}\mathbb{B}_2(\varepsilon) = \displaystyle\int_0^x \frac{\langle \gamma'(s), \varphi'(s)\rangle}{|\gamma'(s)+\varepsilon\varphi'(s)|}\,\mathrm{d}s + \int_y^1 \frac{\langle \gamma'(s), \varphi'(s)\rangle}{|\gamma'(s)+\varepsilon\varphi'(s)|}\,\mathrm{d}s & \text{if } \mathbb{B}_2(\varepsilon) < \mathbb{B}_1(\varepsilon) \end{cases} \\
&\quad = \chi_{\{\mathbb{B}_1(\varepsilon)<\mathbb{B}_2(\varepsilon)\}} \int_x^y \frac{\langle \gamma'(s), \varphi'(s)\rangle}{|\gamma'(s)+\varepsilon\varphi'(s)|}\,\mathrm{d}s \\
&\qquad + \chi_{\{\mathbb{B}_2(\varepsilon)<\mathbb{B}_1(\varepsilon)\}} \left(\int_0^x \frac{\langle \gamma'(s), \varphi'(s)\rangle}{|\gamma'(s)+\varepsilon\varphi'(s)|}\,\mathrm{d}s + \int_y^1 \frac{\langle \gamma'(s), \varphi'(s)\rangle}{|\gamma'(s)+\varepsilon\varphi'(s)|}\,\mathrm{d}s \right)
\end{aligned}$$

where χ is the characteristic function. This can be made rigorous using mollification of the characteristic functions,to smooth them so that the derivatives are well defined, then taking limits gives the above. We then set $\varepsilon = 0$ and the chain rule

yields that

$$\mathbb{B}\colon \quad \frac{\mathrm{d}}{\mathrm{d}\varepsilon}\frac{1}{(\min\{\mathbb{B}_1(\varepsilon),\mathbb{B}_2(\varepsilon)\})^2}\Big|_{\varepsilon=0}$$

$$= \begin{cases} -2\dfrac{\int_x^y \frac{\langle\gamma'(s),\varphi'(s)\rangle}{|\gamma'(s)|}\,\mathrm{d}s}{\left(\int_x^y \gamma'(s)\,\mathrm{d}s\right)^3} & \text{if } \mathbb{B}_1(0) < \mathbb{B}_2(0) \\ -2\dfrac{\left(\int_0^x \frac{\langle\gamma'(s),\varphi'(s)\rangle}{|\gamma'(s)|}\,\mathrm{d}s + \int_y^1 \frac{\langle\gamma'(s),\varphi'(s)\rangle}{|\gamma'(s)|}\,\mathrm{d}s\right)}{\left(\int_0^x \gamma'(s)\,\mathrm{d}s + \int_y^1 \gamma'(s)\,\mathrm{d}s\right)^3} & \text{if } \mathbb{B}_2(0) < \mathbb{B}_1(0) \end{cases}$$

$$=: -2F_{\gamma,\varphi}(x,y)$$

Overall, we combine our forms for $\mathbb{A}, \mathbb{B}, \mathbb{C}$:

$$\langle \delta E(\gamma), \varphi\rangle = \iint_{[0,1]^2} -2\left(\frac{\langle\gamma(x)-\gamma(y),\varphi(x)-\varphi(y)\rangle}{|\gamma(x)-\gamma(y)|^4} - F_{\gamma,\varphi}(x,y)\right)|\gamma'(x)||\gamma'(y)| + \left(\frac{1}{|\gamma(x)-\gamma(y)|^2} - \frac{1}{d_\gamma(x,y)^2}\right)\left(\frac{\langle\gamma'(x),\varphi'(x)\rangle}{|\gamma'(x)|}|\gamma'(y)| + \frac{\langle\gamma'(y),\varphi'(y)\rangle}{|\gamma'(y)|}|\gamma'(x)|\right)\mathrm{d}x\,\mathrm{d}y \tag{7.1}$$

Remark. We also gain from this a simple identity: $\langle \delta E(\gamma), \gamma\rangle = 0$

Remark. We do not proceed in detail through the discretisation, but one may employ the 2 dimensional midpoint rule with a tensor ansatz, and discrete geodesic distance of a degree 1 polynomial approximation Γ_N of Γ parameterised by $P_N : [0,1] \to \Gamma_N$ as seen throughout this paper.

7.2 Numerical results

We implement (7.1) the above formula for the energy variation as a force in the BGN scheme. This is acheived by including it as an explicit term in the right hand side of the equation of Problem 5.2.3:

$$\begin{cases} \displaystyle\int_I \frac{x_h^n - x_h^{n-1}}{\tau}\cdot {x_{h\theta}^{\perp}}^{n-1}\psi_h - \kappa_h^n\psi_h|x_{h\theta}^{n-1}|\,\mathrm{d}\theta &= \displaystyle\int_I f(c_h^{n-1})\psi_h|x_{h\theta}^{n-1}|\,\mathrm{d}\theta - \langle\delta E(x_h^{n-1}),\psi_h\rangle \\ \displaystyle\int_I \kappa_h^n\phi_h\cdot {x_{h\theta}^{\perp}}^{n-1} + \frac{(x_{h\theta}^n - x_{h\theta}^{n-1})\cdot\phi_{h\theta}}{|x_{h\theta}^{n-1}|}\,\mathrm{d}\theta &= -\displaystyle\int_I \frac{x_{h\theta}^{n-1}\cdot\phi_{h\theta}}{|x_{h\theta}^{n-1}|}\,\mathrm{d}\theta \end{cases}$$

Thus with the surface finite elements we are required to evaluate the above form for every basis function ϕ_j, $\forall j = 1, \ldots, N$. and follow through the implementation as before. We approximate the geodesic and Euclidean distances as previously discussed in this project.

As an extension of the project, we were unable to implement cutoffs and smoothing to this new system, we implement the original discrete mobius energy that is set to 0 on the diagonal (in a similar way to Scholtes's energy) as an engineering solution, as we have already seen that this area has little effect. The numerics below demonstrate the effect of this esnergy at timestep 1, 150 and 500 (chosen for behavioural significance). The step size is on the order of 10^{-9}, far smaller than in previous implementation to retain stability which was affected by the new forcing terms. We suspect due to the equidistribution, when neighbouring points are very close and are subjected to forces based on the energy, which is only loosely coupled to the scheme, they may be pushed past one another. The following have $N = 140$, $a = 3$, $r = 0.7$, $\theta = \pi + 2.3$.

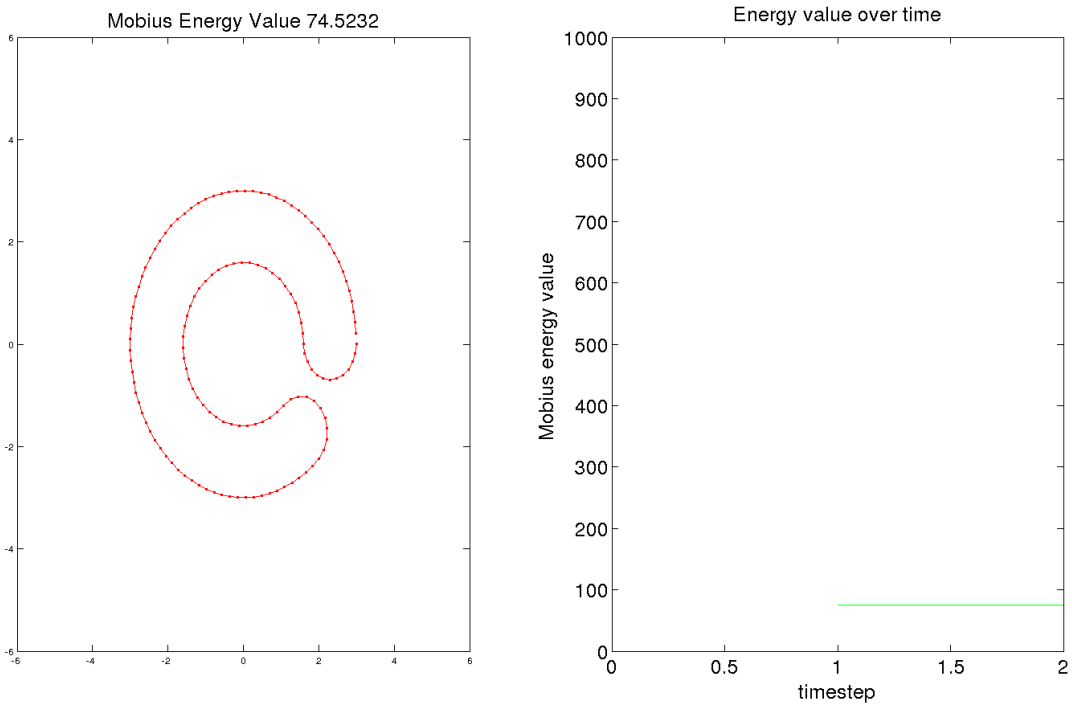

Figure 7.1: *The mesh distribution in early timesteps.*

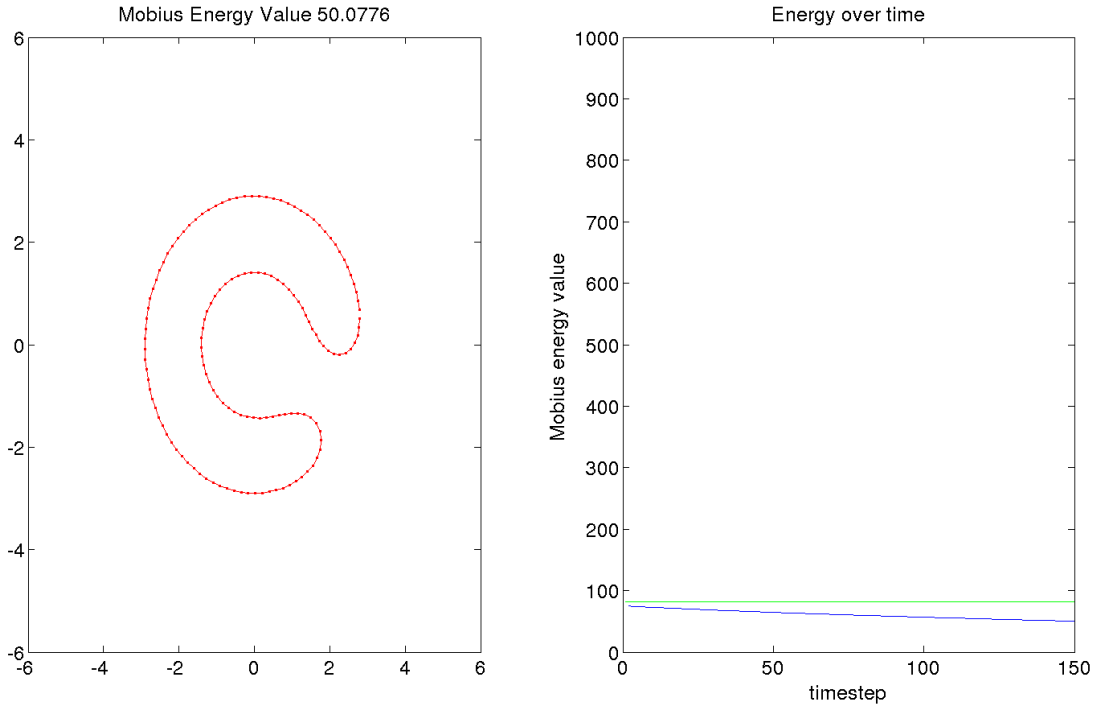

Figure 7.2: *The mesh distribution at timestep 150*

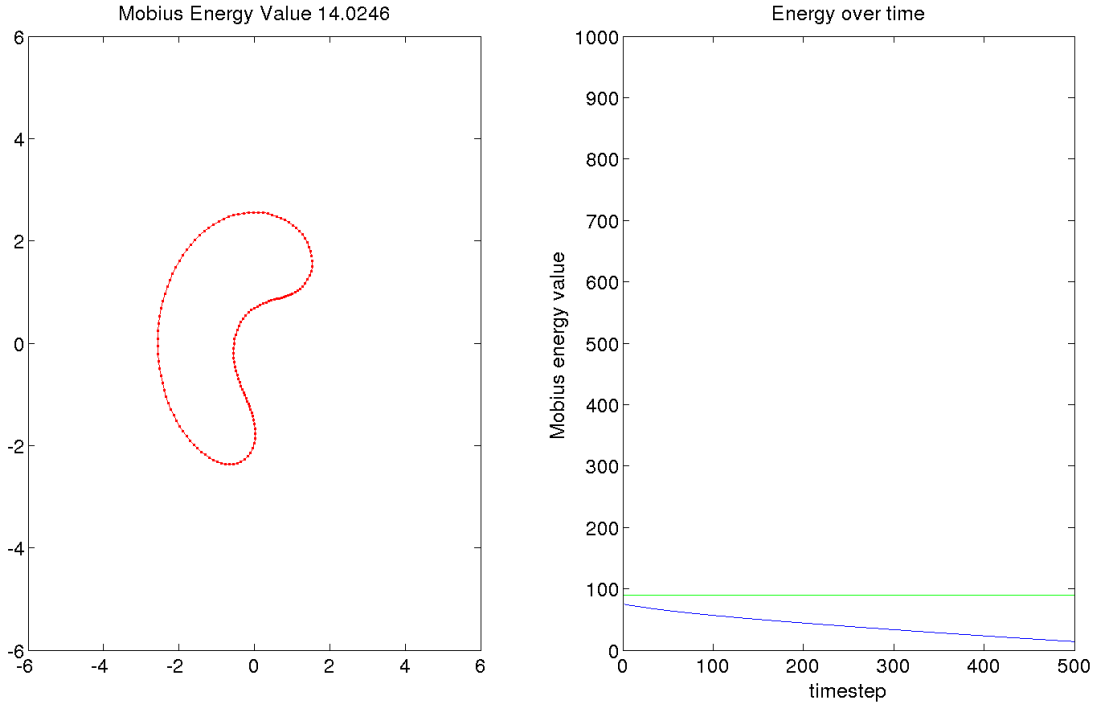

Figure 7.3: *The mesh distribution at timestep 500.*

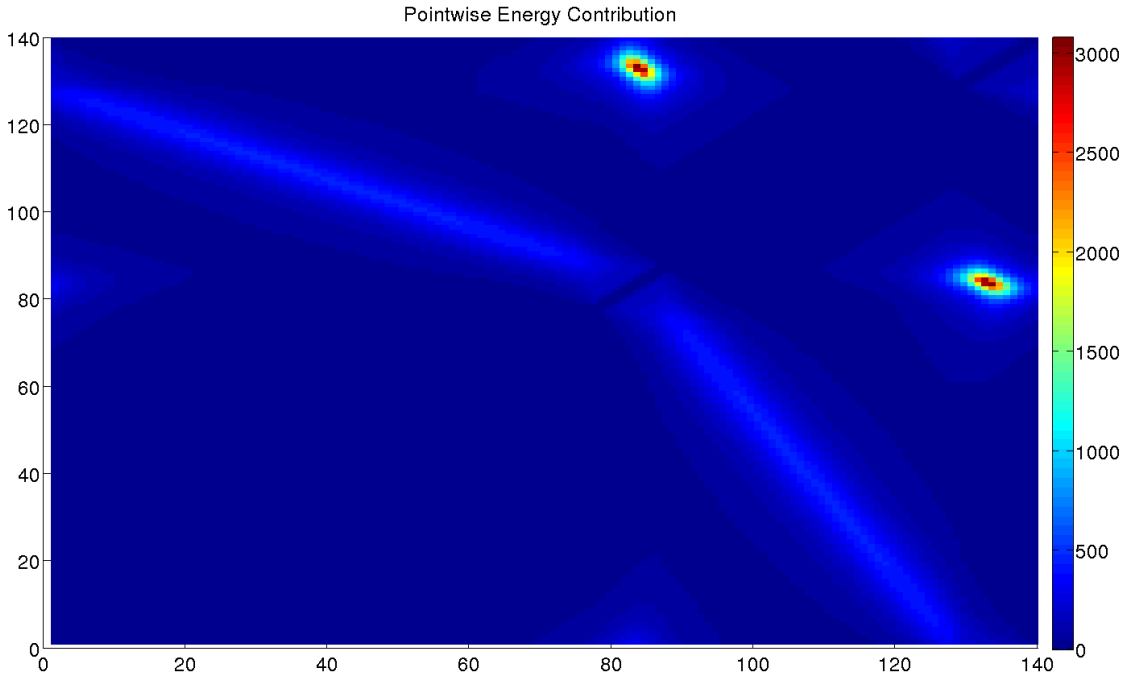

Figure 7.4: *The energy density in early timesteps.*

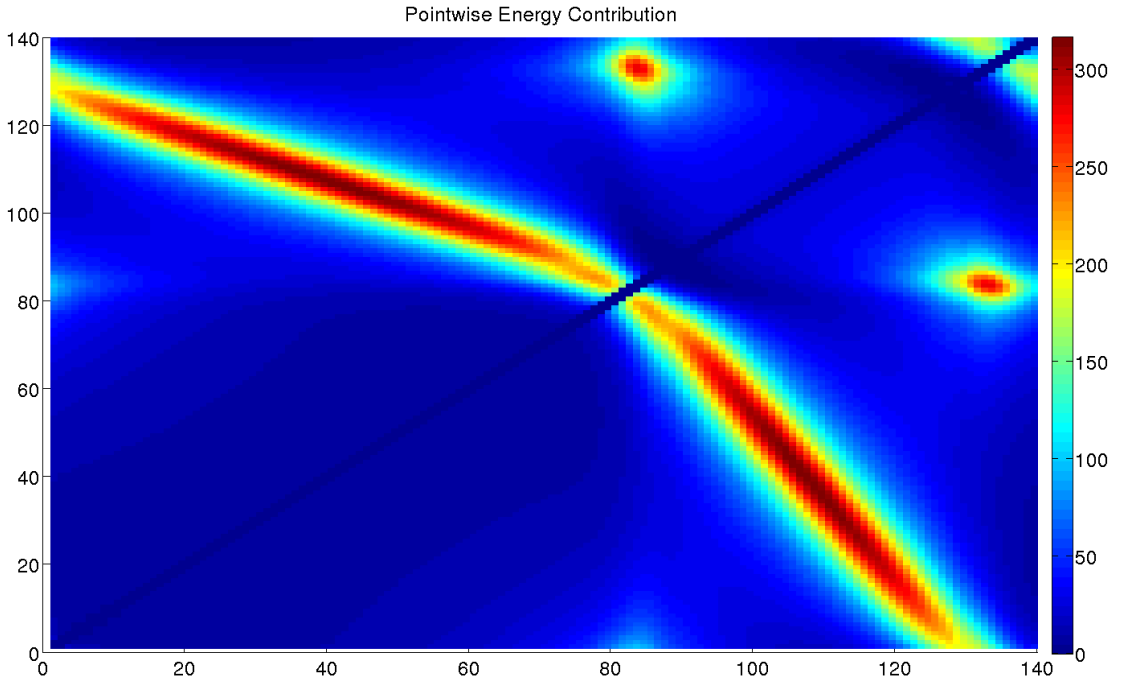

Figure 7.5: *The energy density at timestep 150.*

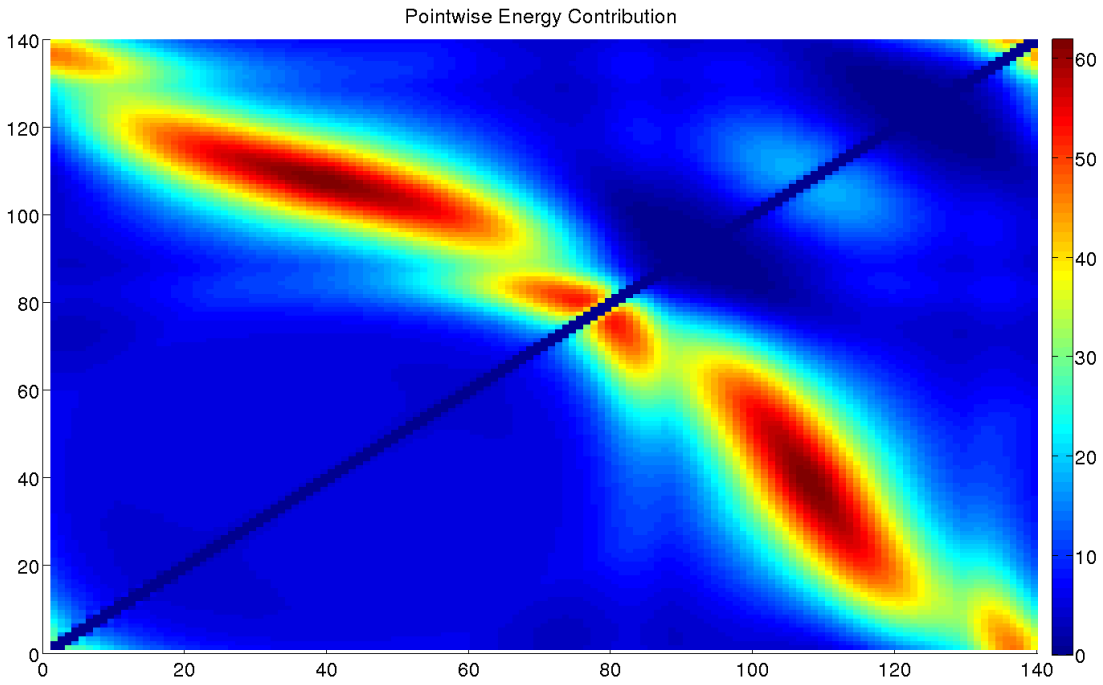

Figure 7.6: *The energy density in at timestep 500.*

From the numerics we observe most importantly that the intersection does not occur despite the previous forcing, and that the new force even pushes the ends away from each other to the extent that the curve shortening flow then governs the motion. In the density graphs we see how at first the two red patches (that represent the ends almost touching) are reduced by timestep 150. Then after timestep 150 the prevailing peak in the energy density is seen as a band that passes across the diagonal (it represents the distance across the width of the cell, from the inner to the outer edges of the 'C'). This is then reduced again by time 500 - making the C shape smoother and more like a circle. The instability would usually start to occur after this formation due to insufficiently small timesteps however in the future one could hope that there are other ways round this problem. This hopefully serves to demonstrate that, with correct and finely tuned implemention and with greater efficiency (which becomes an issue once again due to the complexity of this function), that this displays the good behaviour which we seek that will prevent intersections in such membranes from occuring.

Chapter 8

Conclusions

To conclude, we have studied in detail the form and convergence of the Möbius energy and its density function. We have found that, given one knows the exact smooth curve, one may use simple quadrature theory to approximate the integral, and this will give you $\mathcal{O}(h)$ convergence. We saw how one could improve upon this by looking by defining $F(x,x) \coloneqq h \lim_{N\to\infty} F(x, x \pm \frac{1}{N})$, or considering a smoothing around this point, this increase obtained $\mathcal{O}(h^2)$ convergence.

Similarly with the discretisation, we first inspected Scholtes energy, which is a reliable starting point. However once again it did not prove to have the correct convergence and relied upon an arclength parametrisation. We generalised this to arbitrary parametrisation, and then again considered the limits $\lim_{N\to\infty} F(a_i, a_i \pm \frac{1}{N})$ for each i. We try two different smoothing methods and find both improve the order to $\mathcal{O}(h^2)$, although this requires a choice the radius of smoothing in each case - of which I have provided one solution for each. We also create some solutions for the efficiency of the methods such as the cleverly chosen cutoff or an equidistribution scheme.

The motivation of this project was the biological membrane motion due to actin, and so we have implemented two different models for this. We see that Dziuk-ESFEM coupling performs well in the short scale for detection of intersections, however the lack of equidistribution which may arise over time can severely affect its effectiveness. The BGN coupling is shown to dominate this scheme at detection in similar scenarios.

We also attempt to use a proportional calculation that is very efficient but only for tight equidistribution, if one can find a good scheme for this equidistribution it may prove far more efficient due to the order reduction of an $\mathcal{O}(h^3)$ complexity down to $\mathcal{O}(h^2)$ for the discrete energy. However the BGN-ALE ESFEM does not

seem quite effective enough, due to the equidistributing flow's proximity to its minimum distribution. We then ensured that none of the cutting off or smoothing procedures improved efficiency and did not effect the models ability to detect intersection in our implementation.

Lastly we presented the implementation for the prevention of self intersections. This demonstrated that the variation could be effectively implemented to prevent intersection, however the computational complexity was inefficient due to the complexity of the equations involved. However by the construction and behaviour of the energy itself before in the paper one could see that some cleverly defined cutoff functions would no doubt be of use, or perhaps more simplified constructions, would be of use.

The analysis of regularity and convergence such energy variation discretisations is also is still open for study. Also at present the increase in dimension to 3 dimensions is open for research and seems highly nontrivial, and of course the further increase in complexity may prove difficult to overcome with this energy in this setting.

Bibliography

[1] John W. Barrett, Harald Garcke, and Robert Nuernberg. A parametric finite element method for fourth order geometric evolution equations. *JOURNAL OF COMPUTATIONAL PHYSICS*, 222(1):441–467, MAR 1 2007.

[2] Simon Blatt. Boundedness and regularizing effects of O'Hara's knot energies. *Journal of Knot Theory and Its Ramifications*, 21(01):1250010, 2012.

[3] Simon Blatt and Philipp Reiter. Does finite knot energy lead to differentiability? *Journal of Knot Theory and Its Ramifications*, 17(10):1281–1310, 2008.

[4] G. Dziuk. An algorithm for evolutionary surfaces. *Numerische Mathematik*, 58(1):603–611, 1990.

[5] G. Dziuk. Convergence of a semi-discrete scheme for the curve shortening flow. *Mathematical Models and Methods in Applied Sciences*, 04(04):589–606, 1994.

[6] G. Dziuk and C. M. Elliott. Finite elements on evolving surfaces. *IMA Journal of Numerical Analysis*, 27(2):262–292, 2007.

[7] Gerhard Dziuk and Charles M. Elliott. Finite element methods for surface pdes. *Acta Numerica*, Volume 22:289–396, May 2013.

[8] Charles M. Elliott, Björn Stinner, and Chandrasekhar Venkataraman. Modelling cell motility and chemotaxis with evolving surface finite elements. *Interface*, 9(76):3027–3044, November 2012.

[9] Charles M. Elliott and Vanessa Styles. An ALE ESFEM for solving pdes on evolving surfaces. *Milan Journal of Mathematics*, 80(2):469–501, 2012.

[10] Michael H. Freedman, Zheng-Xu He, and Zhenghan Wang. Mobius energy of knots and unknots. *Annals of Mathematics*, 139(1):pp. 1–50, 1994.

[11] A Kurganov and S Tsynkov. On spectral accuracy of quadrature formulae based on piecewise polynomial interpolations. *Center for Research in Scientific*

Computation, North Carolina State University, Technical Report No. CRSC-TR07-11, 2007.

[12] Alexander Kurganov and Jeffrey Rauch. The order of accuracy of quadrature formulae for periodic functions. In *Advances in Phase Space Analysis of Partial Differential Equations*, pages 155–159. Springer, 2009.

[13] Ruo Li, Tao Tang, and Pingwen Zhang. Moving mesh methods in multiple dimensions based on harmonic maps. *Journal of Computational Physics*, 170(2):562 – 588, 2001.

[14] Jun O'Hara. Family of energy functionals of knots. *Topology and its Applications*, 48(2):147 – 161, 1992.

[15] Jun OHara. Energy of a knot. *Topology*, 30(2):241 – 247, 1991.

[16] QaziI. Rahman and Gerhard Schmeisser. Characterization of the speed of convergence of the trapezoidal rule. *Numerische Mathematik*, 57(1):123–138, 1990.

[17] Eric J. Rawdon and Jonathan K. Simon. Polygonal approximation and energy of smooth knots. *Journal of Knot Theory and Its Ramifications*, 15(04):429–451, 2006.

[18] Sebastian Scholtes. Discrete Möbius energy. *arXiv:1311.3056v1*, 2013.

Chapter 9

Appendix

Simpson's quadrature

The Simpson's quadrature rule is given by $\int_a^b f(x)\,\mathrm{d}x \approx \frac{b-a}{6}\left(f(a)+4f(\frac{a+b}{2})+f(b)\right)$, Thus we obtain:

$$
\begin{aligned}
&\int_{a_j}^{a_{j+1}}\int_{a_i}^{a_{i+1}} F(x,y)\,\mathrm{d}x\,\mathrm{d}y \\
&= \int_{a_j}^{a_{j+1}} \frac{a_{i+1}-a_i}{6}\left(F(a_i,y)+4F\left(\frac{a_i+a_{i+1}}{2},y\right)+F(a_{i+1},y)\right)\mathrm{d}y \\
&= \frac{(a_{i+1}-a_i)(a_{j+1}-a_j)}{36}\Bigg[\left(F(a_i,a_j)+4F\Big(\frac{a_i+a_{i+1}}{2},a_j\Big)+F(a_{i+1},a_j)\right) \\
&+4\left(F\Big(a_i,\frac{a_j+a_{j+1}}{2}\Big)+4F\Big(\frac{a_i+a_{i+1}}{2},\frac{a_j+a_{j+1}}{2}\Big)+F\Big(a_{i+1},\frac{a_j+a_{j+1}}{2}\Big)\right) \\
&\qquad\qquad +\left(F(a_i,a_{j+1})+4F\Big(\frac{a_i+a_{i+1}}{2},a_{j+1}\Big)+F(a_{i+1},a_{j+1})\right)\Bigg] \\
&=: (a_{i+1}-a_i)(a_{j+1}-a_j)G(a_i,a_j)
\end{aligned}
$$

Once again, if we define the point $a_{N+1} \coloneqq a_1$ we can represent the discretised integral as

$$I_N(F) = \frac{1}{36N^2}\sum_{i,j=1}^{N} G(a_i,a_j)$$

The error term associated to this composite simpsons rule over an interval $[a,b]$ with meshsize h is given by a term $-\frac{1}{180}(b-a)h^4 f^{(4)}(\xi)$ (with $\xi \in (a,b)$).

Limit point of the integrand $F(x,x)$ of the continuous Möbius energy

We show that for $F(x,y)$ the continuous integrand of our energy and letting $y \to x$, due to invariance under rotations and translations on the unit circle we consider $x = 0$, and we can take $0 < y \ll 1$. We have shown previously in Section 2.2.2 that

$$|\gamma(a_k) - \gamma(0)|^2 - d_\gamma(a_k, 0)^2 = -\frac{4\pi^4 k^4}{3N^4} + \mathcal{O}\Big(\frac{1}{N^6}\Big)$$

and so - anywhere in the unit circle we have $|\gamma'(x)| = 2\pi$:

$$\begin{aligned}
F(a_k, 0) &= 4\pi^2 \left(\frac{1}{|\gamma(a_k) - \gamma(0)|^2} - \frac{1}{d_\gamma(a_k,0)^2} \right) \\
&= 4\pi^2 \left(\frac{d_\gamma(a_k,0)^2 - |\gamma(a_k) - \gamma(0)|^2}{d_\gamma(a_k,0)^2 |\gamma(a_k) - \gamma(0)|^2} \right) \\
&= -4\pi^2 \left(-\frac{4\pi^4 k^4}{3N^4} + \mathcal{O}\Big(\frac{1}{N^6}\Big) \right) \frac{N^2}{4\pi^2 k^2 \cdot (\frac{4\pi^2 k^2}{N^2} - \frac{4\pi^4 k^4}{3N^4} + \mathcal{O}(\frac{1}{N^6}))} \\
&= \left(\frac{16\pi^6 k^4}{3N^4} + \mathcal{O}\Big(\frac{1}{N^6}\Big) \right) \frac{N^4}{16\pi^4 k^4 \cdot (1 - \frac{\pi^2 k^2}{3N^2} + \mathcal{O}(\frac{1}{N^4}))} \\
&= \frac{\frac{\pi^2}{3} + \mathcal{O}(\frac{1}{N^2})}{1 - \frac{\pi^2 k^2}{3N^2} + \mathcal{O}(\frac{1}{N^4})}
\end{aligned}$$

We now apply the power series $\frac{1}{1-x} = 1 + x + \mathcal{O}(x^2)$

$$\begin{aligned}
&= \Big(\frac{\pi^2}{3} + \mathcal{O}\Big(\frac{1}{N^2}\Big) \Big) \Big(1 + \frac{\pi^2 k^2}{3N^2} + \mathcal{O}\Big(\frac{1}{N^4}\Big) \Big) \\
&= \frac{\pi^2}{3} + \frac{\pi^4 k^4}{9N^2} + \mathcal{O}\Big(\frac{1}{N^6}\Big)
\end{aligned}$$

So setting $k = 0$ yields a natural limit for $F(x,x) = \frac{\pi^2}{3}$ will be the natural limit for this function

Behaviour of the integrand $F(x,y)$ of the discrete Möbius energy for $|p_N(x) - p_N(y)| \ll 1$

We show that for $F(x,y)$ the discrete integrand of our energy and taking y close to x. Due to invariance under rotations and translations on the unit circle we consider $x = 0$, and we can take $0 < y \ll 1$. We have shown previously in Section 2.3.2 that

$$|p_N(a_k) - p_N(0)|^2 - d_N(a_k, 0)^2 = \frac{4\pi^4 k^2 (1 - k^2)}{3N^4} + \mathcal{O}\Big(\frac{1}{N^6}\Big)$$

Thus, as $|\partial'_N(a_k)| = 2\pi \ \forall\, k$ in the approximated circle (using our discrete derivative formula):

$$
\begin{aligned}
&F_N(a_k, 0) \\
&= 4\pi^2 \left(\frac{1}{|p_N(a_k) - p_N(0)|^2} - \frac{1}{d_N(a_k,0)^2} \right) \\
&= 4\pi^2 \left(\frac{d_N(a_k,0)^2 - |p_N(a_k) - p_N(0)|^2}{d_N(a_k,0)^2 |p_N(a_k) - p_N(0)|^2} \right) \\
&= -4\pi^2 \left(\frac{4\pi^4 k^2 (1-k^2)}{3N^4} + \mathcal{O}\Big(\frac{1}{N^6}\Big) \right) \cdot \frac{1}{\big(\frac{4\pi^2 k^2}{N^2} - \frac{4\pi^4 k^2}{3N^4} + \mathcal{O}(\frac{1}{N^6})\big)\big(\frac{4\pi^2 k^2}{N^2} - \frac{4\pi^4 k^4}{3N^4} + \mathcal{O}(\frac{1}{N^6})\big)} \\
&= \left(\frac{16\pi^6 k^2 (k^2-1)}{3N^4} + \mathcal{O}\Big(\frac{1}{N^6}\Big) \right) \cdot \frac{N^4}{16k^4\pi^4 \big(1 - \frac{\pi^2}{3N^2} + \mathcal{O}(\frac{1}{N^4})\big)\big(1 - \frac{2\pi^2 k^2}{3N^2} + \mathcal{O}(\frac{1}{N^4})\big)} \\
&= \frac{\frac{\pi^2(k^2-1)}{3} + \mathcal{O}(\frac{1}{N^2})}{k^2\big(1 - \frac{\pi^2(k^2+1)}{3N^2} + \mathcal{O}(\frac{1}{N^4})\big)}
\end{aligned}
$$

We now apply the power series $\frac{1}{1-x} = 1 + x + \mathcal{O}(x^2)$

$$
\begin{aligned}
&= \frac{1}{k^2}\Big(\frac{\pi^2(k^2-1)}{3} + \mathcal{O}(\frac{1}{N^2})\Big)\Big(1 - \frac{\pi^2(k^2+1)}{3N^2} + \mathcal{O}(\frac{1}{N^4})\Big) \\
&= \frac{\pi^2(k^2-1)}{3k^2} + \mathcal{O}(\frac{1}{N^2})
\end{aligned}
$$

so we let $N \to \infty$ and obtain a discrete limiting curve of $F(a_k, 0) = \frac{\pi^2(k^2-1)}{3k^2}$. If we let $|k|$ become large then this will converge towards $\frac{\pi^2}{3}$.

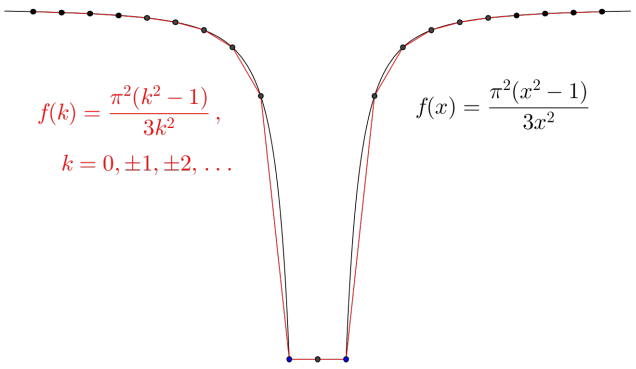

Figure 9.1: *Shows for $k = 0, \pm 1, \pm 2, \ldots$ and for N large, the behaviour of F_N where $|p_N(x) - p_N(y)| \ll 1$*

Gauss-Green formula

The hypersurface $\Gamma = \{\Gamma(t)\}_t$ with given material velocity $v\colon (0,T)\times\Gamma \to \mathbb{R}^2$, where $\mathcal{G} = \{(t,\Gamma(t))|t \in [0,T]\}$

$$\int_\Gamma \nabla_\Gamma f \,\mathrm{d}\mathcal{H}^{n-1} = -\int_\Gamma f\boldsymbol{\kappa}\,\mathrm{d}\mathcal{H}^{n-1} + \int_{\partial\Gamma} f\boldsymbol{\mu}\,\mathrm{d}\mathcal{H}^{n-2} \tag{9.1}$$

Transport identity

$$\frac{\mathrm{d}}{\mathrm{d}t}\int_{\Gamma(\cdot)} f(\cdot,x)\,\mathrm{d}\mathcal{H}^{n-1}(x)\Big|_t = \int_{\Gamma(t)} (\partial_t^\bullet f(t,x) + f(t,x)\nabla_{\Gamma(t)}\cdot v(t,x))\,\mathrm{d}\mathcal{H}^{n-1}(x) \tag{9.2}$$

Divergence Theorem for surfaces

$$\int_{\Gamma(t)} \nabla_{\Gamma(t)}\cdot v\,\mathrm{d}\mathcal{H}^{n-1} = -\int_{\Gamma(t)} v\cdot\boldsymbol{\kappa}\,\mathrm{d}\mathcal{H}^{n-1} + \int_{\partial\Gamma(t)} v\cdot\boldsymbol{\mu}\,\mathrm{d}\mathcal{H}^{n-2} \tag{9.3}$$

Proof. We define $\partial_{i_{\Gamma(t)}} f \coloneqq \partial_i f - (\nabla f\cdot\boldsymbol{\nu})\boldsymbol{\nu}_i = (\nabla_{\Gamma(t)} f)\cdot\boldsymbol{e}_i$. Then, we use Gauss-Green formula to show

$$\begin{aligned}
\int_{\Gamma(t)} \nabla_{\Gamma(t)}\cdot v\,\mathrm{d}\mathcal{H}^{n-1} &= \int_{\Gamma(t)} \mathrm{tr}\Big(\{\partial_{i_{\Gamma(t)}} v_j\}_{ij}\Big)\,\mathrm{d}\mathcal{H}^{n-1}\\
&= \sum_{i=1}^n \int_{\Gamma(t)} (\nabla_{\Gamma(t)} v_i)\cdot\boldsymbol{e}_i\,\mathrm{d}\mathcal{H}^{n-1}\\
&\overset{(9.1)}{=} -\sum_{i=1}^n \int_{\Gamma(t)} (v_i\boldsymbol{\kappa})\cdot\boldsymbol{e}_i\,\mathrm{d}\mathcal{H}^{n-1} + \sum_{i=1}^n \int_{\Gamma(t)} (v_i\boldsymbol{\mu})\cdot\boldsymbol{e}_i\,\mathrm{d}\mathcal{H}^{n-2}
\end{aligned}$$

$$\begin{aligned}
&= -\sum_{i=1}^n \int_{\Gamma(t)} v_i\boldsymbol{\kappa}_i\,\mathrm{d}\mathcal{H}^{n-1} + \sum_{i=1}^n \int_{\Gamma(t)} v_i\boldsymbol{\mu}_i\,\mathrm{d}\mathcal{H}^{n-2}\\
&= -\int_{\Gamma(t)} (v\cdot\boldsymbol{\kappa})\,\mathrm{d}\mathcal{H}^{n-1} + \int_{\Gamma(t)} v\cdot\boldsymbol{\mu}\,\mathrm{d}\mathcal{H}^{n-2}
\end{aligned}$$

□

Derivation of Weak form of the surface PDE

(For the sake of notation we now drop the t in $\nabla_{\Gamma(t)}$ and $\Gamma(t)$.)
Now we have obtained the strong form, we seek a weak form to derive the estimates we require. Firstly recall the Neumann boundary conditions $q(t)\cdot\boldsymbol{\mu}(t) = g(t)$ on

$\partial\Gamma(t)$ and initial data $u(0,x) = u_0(x)$, with $u_0 \colon \Gamma(0) \to \mathbb{R}$. For any test function $\varphi \colon \Gamma \to \mathbb{R}$

$$\begin{aligned}
\int_\Gamma f\varphi \,\mathrm{d}\mathcal{H}^{n-1} &= \int_\Gamma (\partial_t^\bullet u + u\nabla_\Gamma \cdot v - D\Delta_\Gamma u)\varphi \,\mathrm{d}\mathcal{H}^{n-1} \\
&= \int_\Gamma \varphi\partial_t^\bullet u + u\varphi\nabla_\Gamma \cdot v + D\nabla_\Gamma u \cdot \nabla_\Gamma\varphi \,\mathrm{d}\mathcal{H}^{n-1} + \int_{\partial\Gamma} g\varphi \,\mathrm{d}\mathcal{H}^{n-2} \\
&= \int_\Gamma \underbrace{(\varphi\partial_t u + u\partial_t\varphi + v\varphi\cdot\nabla u}_{=\partial_t(\varphi u)+v\cdot\nabla(\varphi u)} + u\varphi\nabla_\Gamma\cdot v) - u\partial_t\varphi - uv\cdot\nabla\varphi \\
&\qquad\qquad + D\nabla_\Gamma u \cdot \nabla_\Gamma\varphi \,\mathrm{d}\mathcal{H}^{n-1} + \int_{\partial\Gamma} g\varphi \,\mathrm{d}\mathcal{H}^{n-2}
\end{aligned}$$

Note that the blue terms come from the product rule $v\varphi\cdot\nabla u + uv\cdot\nabla\varphi = v\cdot\nabla(\varphi u)$. Continuing, we have

$$\begin{aligned}
\int_\Gamma f\varphi \,\mathrm{d}\mathcal{H}^{n-1} &= \int_\Gamma \underbrace{(\partial_t^\bullet(u\varphi) + u\varphi\nabla_\Gamma\cdot v)}_{\text{(transport identity)}} - \underbrace{(u\partial_t\varphi + uv\cdot\nabla\varphi)}_{=u\partial_t^\bullet\varphi} \\
&\qquad\qquad + D\nabla_\Gamma u\cdot\nabla_\Gamma\varphi \,\mathrm{d}\mathcal{H}^{n-1} + \int_{\partial\Gamma} g\varphi \,\mathrm{d}\mathcal{H}^{n-2} \\
&\overset{(9.2)}{=} \frac{\mathrm{d}}{\mathrm{d}t}\Big(\int_\Gamma u\varphi \,\mathrm{d}\mathcal{H}^{n-1}\Big) + \int_\Gamma -u\partial_t^\bullet\varphi + D\nabla_\Gamma u\cdot\nabla_\Gamma\varphi \,\mathrm{d}\mathcal{H}^{n-1} + \int_{\partial\Gamma} g\varphi \,\mathrm{d}\mathcal{H}^{n-2}
\end{aligned}$$

Which is a weak form of the PDE we wish to look at.

Explicit mass lumping for linear SFEM

For each $i = 1, \ldots, N$ consider a particular basis function:

$$\begin{aligned}
\int_0^1 b_i(\theta)|x_{h\theta}| \,\mathrm{d}\theta &= \int_{\theta_{i-1}}^{\theta_i} \frac{\theta-\theta_{i-1}}{\theta_i-\theta_{i-1}} N \underbrace{|x_i - x_{i-1}|}_{q_i} \,\mathrm{d}\theta + \int_{\theta_i}^{\theta_{i+1}} \frac{\theta_{i+1}-\theta}{\theta_{i+1}-\theta_i} N \underbrace{|x_{i+1}-x_i|}_{q_{i+1}} \,\mathrm{d}\theta \\
&= \frac{1}{2}N^2 q_i \,(\theta-\theta_{i-1})^2\big|_{\theta_{i-1}}^{\theta_i} + \frac{1}{2}N^2 q_{i+1}\,(\theta_{i+1}-\theta)^2\big|_{\theta_i}^{\theta_{i+1}} \\
&= \frac{1}{2}(q_i + q_{i+1})
\end{aligned}$$

For $u_h(\theta) = x_h(\theta)$. Firstly let $x_i = x(\theta_i)$, $\forall i$, then

$$x_h(\theta)|_{(\theta_{i-1},\theta_i)} = \frac{\theta-\theta_{i-1}}{\theta_i-\theta_{i-1}}x_i + \frac{\theta_i-\theta}{\theta_i-\theta_{i-1}}x_{i-1}, \qquad x_{h\theta}|_{(\theta_{i-1},\theta_i)} = \frac{x_i-x_{i-1}}{\theta_i-\theta_{i-1}}$$

Previously this would need to be incorporated into the integral calculation. Now however we merely multiply $x_i(\frac{1}{2}(q_i + q_{i+1}))$.

Similarly we may apply to the RHS to obtain the form with $u_h = f(c_h)$,thus $u_i = f(c_i)$ and knowing

$$x_{h\theta}^{\perp}\Big|_{(\theta_{i-1},\theta_i)} = \frac{(x_i - x_{i-1})^{\perp}}{\theta_i - \theta_{i-1}} = \begin{pmatrix} 0 & -1 \\ 1 & 0 \end{pmatrix} \frac{x_i - x_{i-1}}{\theta_i - \theta_{i-1}}$$

Parametrisations for numerical test shapes

The unit circle

$$\gamma(t) = \begin{pmatrix} \sin(2\pi t) \\ \cos(2\pi t) \end{pmatrix} \qquad \forall\, t \in [0,1]$$

The ellipsoid

$$\gamma(t) = \begin{pmatrix} 2\sin(2\pi t) \\ 0.8\cos(2\pi t) \end{pmatrix} \qquad \forall\, t \in [0,1]$$

The "C-shape", for r, a, $\theta > 0$, and $L = 2a\theta + 2r(\pi - \theta)$ the total arclength let

$$\begin{aligned} L_1 &= \frac{a\theta}{L} \\ L_2 &= \frac{a\theta + r\pi}{L} \\ L_3 &= \frac{(2a-2r)\theta + r\pi}{L} \end{aligned}$$

$$\gamma(t) = \begin{cases} (a\cos(\frac{Lt}{a}), a\sin(\frac{Lt}{a})) & \forall t \in [0, L_1] \\ (r\cos(\frac{tL}{r} - \frac{(a-r)\theta}{r}) + (a-r)\cos(\theta), r\sin(\frac{tL}{r} - \frac{(a-r)\theta}{r}) + (a-r)\sin(\theta)) & \forall t \in [L_1, L_2] \\ ((a-2r)\cos(\frac{tL}{2a-r} - \frac{r(\pi+\theta)-a\theta}{2a-r}), (a-2r)\sin(\frac{tL}{2a-r} - \frac{r(\pi+\theta)-a\theta}{2a-r})) & \forall t \in [L_2, L_3] \\ r\cos(\frac{tL}{r} - \frac{2(a-r)\theta}{r}) + (a-r), r\sin(\frac{tL}{r} - \frac{2(a-r)\theta}{r}) & \forall t \in [L_3, 1] \end{cases}$$

Estimated Order of convergence

We calculate our EOC based on the values of the energy functional E at certain grid sizes. As we do not know what the limiting energy is in some cases we use a formula that does not require an exact solution, the penalty is that for any grid size h, the values of $E(2h)$ and $E(\frac{h}{2})$ must be known for the calculation.

$$\mathrm{EOC}(h) = \log_2\left(\frac{E(2h) - E(h)}{E(h) - E(\frac{h}{2})}\right)$$

for example $E(h) \sim Ch^p$ (i.e order 2) then,

$$EOC(h) = \log_2 \left(\frac{2^p Ch^2 - Ch^2}{Ch^2 - \frac{C}{2^p} h^2} \right) = \log_2 \left(\frac{2^p - 1}{1 - \frac{1}{2^p}} \right) = \log_2(2^p) = p$$